REFLECTORS IN UPPER MANTLE ABOVE THE DEEP EARTHQUAKES

by
Ming Te Lin
B.E., Chung Cheng Institute of Technology
(1965)
M.S., National Central University
(1970)

SUBMITTED IN
PARTIAL FULFILLMENT
OF THE REQUIREMENTS FOR THE
DEGREE OF MASTER OF SCIENCE
at the
MASSACHUSETTS INSTITUTE OF
TECHNOLOGY
June, 1974

Signature of Author.....
Department of Earth and Planetary Sciences

Certified by.....
Thesis Supervisor

Accepted by.....
Chairman, Departmental Committee
on Graduate Students

ABSTRACT

REFLECTORS IN UPPER MANTLE ABOVE THE DEEP EARTHQUAKES

by

Ming Te Lin

Submitted to the Department of Earth
and Planetary Sciences on June 17, 1974
in partial fulfillment of the
requirements for the degree of
Master of Science

Precursors to pP of deep earthquakes in South America, the Sea of Okhotsk, the Bonin Islands, the New Hebrides and the Fiji-Tonga Islands are studied from LASA, NORSAR, and WWSSN records. These precursors are interpreted as reflections from boundaries in the upper mantle above the deep earthquake sources. The suggested reflectors are ranging in depth from: 100 - 140 km, 240 - 260 km, 280 - 320 km, 340 - 400 km in South America; 80 - 140 km, 220 - 290 km, 320 - 400 km in Sea of Okhotsk; 100 - 130 km, 160 - 200 km, 230 - 260 km, 300 - 330 km, 350 - 400 km in Borin Islands and 110 - 140 km, 160 - 180 km, 230 - 260 km, 280 - 310 km, 330 - 400 km in Fiji-Tonga and New Hebrides region.

Amplitude ratio studies show higher velocity gradients

at the bottom of the low velocity zone. However, the other reflectors suggest 8-10% velocity change on the average. This high velocity gradient beneath the low velocity zone is considered to be the onset of solid solution pyroxene to garnet and the olivine to spinel phase transformation. The boundaries between 230 and 400 km in certain regions correlate with the gaps in the distribution of seismicity with depth. It suggests that the upper and lower parts of the lithosphere are detached, and that the discontinuities between 230 and 350 km might extend to a few hundred kilometers horizontally.

Thesis Supervisor: Keitti Aki
Professor of Geophysics

Dr. John Filson

Staff Scientists
Lincoln Laboratory

Acknowledgements

I would like to express my profound thanks to my advisor, Dr. John Filson, who suggested this study, advised me at critical steps, and corrected the manuscript. I am also deeply indebted to Professor Ketti Aki for his advice and guidance.

Thanks are due to the people of Lincoln Laboratory (seismic discrimination group) for permitting me to use the facilities and helping me in analyzing the data.

I am also grateful to Miss Dorthy Frank for typing this dissertation.

This research was supported by the National Science Council, Republic of China.

Table of Contents

Chapter I

Introduction

Seismic wave studies have contributed greatly to our understanding of the earth's interior. Early works on the interpretation of arrival times of body waves provided much information about the velocity distribution and major divisions in the earth's mantle and core. In the exploration of upper mantle structure, the reflected seismic waves near the earth's surface have long been used. It was Gutenberg (1960) who first noted that the small arrivals preceeding the main group phases of pP, PP, P'P' (PKPPKP) were probably due to the reflections from the Moho or other discontinuities beneath the earth's surface, but he also pointed out difficulties in the interpretation of such arrivals because of the uncertainties in travel times.

Following this, the studies of upper mantle discontinuities by slowness were in two major directions; namely the precursors to PP and the precursors to P'P'. Bolt, O'Neill and Qamar (1968) discussed the former in the $105° < \Delta < 110°$ region; those waves were attributed to the reflections of the PP type from the lower side of the discontinuities in the mantle and were designated PdP where d denotes the depth of reflection. Wright and Muirhead (1969), using nuclear explosion data and array analysis, found that the slowness of precursors to PP were slightly larger than those for P. (Other reports from Bolt (1970), Bolt and Qamar (1969), and

recent models of the upper mantle structure for both P and S waves such as Johnson (1967), Kanamori (1967) and Wright (1970b) have established the presence of two high velocity gradients at depths of about 400 km and 650 km beneath the earth's surface.) However, Angoran (1972) analyzed these precursors, by using beam forming and Vespa analysis of LASA records. He found no convincing evidence for PdP arrivals. Similarly, Wright (1972) measured the azimuths and slowness for coherent signals arriving between P and pp and up to 60 seconds after pp on Yellowknife array records at distances between 90° and 115°. He found no conclusive evidence for PdP waves. Thus, the results of Angoran and Wright might suggest that the discontinuities are only regional phenomena.

The precursors to P'P' have also been investigated extensively and interpreted in terms of reflections. Adams (1968) indicated P'P' precursors as reflections arriving up to 70 sec before the main phase. Although SKKKP phase has been misread as Engdahl and Flinn (1969a) have pointed out, the remaining readings indicated discontinuities at 65 to 70 km, and 160 to 180 km in depth. Engdahl and Flinn (1969b), Adams (1971), Bolt and Qamar (1972) independently found strong evidence of P'P' precursors, P'dP', reflected at 650 km. Moreover, Whitcomb and Anderson (1970) reported that the strongest reflections are from a depth of 630 km

which coincides with the results of others. Other reflectors were found at depths of 280, 520, 950, and 410 km (very weak). The 280 km discontinuities are most interesting because the anomalous change is absent in the recent P wave velocity models. However, Simpson, Wright and Cleary (1971) also showed this discontinuity in their report.

Another approach of these precursors was suggested by Husebye and Madariaga (1970). They interpreted a different kind of mantle reflection involving two reflections, one at the upper side of the discontinuity and one at the free surface. Davies, Kelly and Filson (1971) called these phases, pdpP; where d is the depth of the reflector in km. They used the Vespa process to find the slowness and azimuth. Gentowski and Kanasewich (1974) used the COVESPA technique to study the P codas of a number of shallow teleseismic events. The results revealed systematic patterns which could be attributed to reflections of P waves off discontinuities in the upper mantle within the depth range of 130 to 170 km, and again at 650 km.

From the above review we know that the possible discontinuities in the upper mantle were at depths of 130∿180 km, 280 km, 360∿420 km, and 630∿650 km. Two of the discontinuities are well accepted as being due to the effect of mineralogical phase transformations. According to a shock wave study reported by Ringwood (1970), the transformation of olivine

through spinel into beta phase would occur at a median depth of 397 km with a width of about 27 km. In the 650 km region, β $(MgFe)_2SiO_4$ transform to strontium plumbate structure would be dominant. These results are consistent with those of the study of seismic precursors.

The ideas of our study came from a completely different source. During the processing of short period arrivals from deep South American earthquakes at LASA, the automatic detection schemes do not always correctly identify the pP depth phase. These schemes interpret an intermediate phase between P and pP as pP and identify the true pP as a second event from the same region. The events were designed with depth less than those given by location schemes using P wave travel time from many stations - for example, USCGS reports. These phases, coherent between subarrays, arrive half way between P and pP and the estimated epicentral distances to LASA are around 70°. For deep earthquakes with depths greater than 500 km, these phases apparently cannot be PcP.

After using the VESPA analysis, we found that the slowness of these precursors lie between those of P and pP. The beam forming results also show a clear intermediate phase between P and pP regardless of the slight difference of slowness between precursors and P and pP phases. Thus, following Whitcomb and Anderson (1970), we introduce the nomenclature pdP where d is the depth of the reflector beneath

the earth's surface.

This thesis will analyze the characteristics of reflectors from the pdP phases and the reflectors from which they arise. Deep earthquakes from South America, the Sea of Okhotsk, Bonin Island, the New Hebrides, and Fiji-Tonga Islands are the five regions we are going to investigate. The main data sources are the digitized records of deep events in LASA and NORSAR; however, WWSSN data from South America and the Sea of Okhotsk were also used. In the following chapters, we will describe the data sources first, and then discuss the method of analysis and the quality of the observations. The interpretation of the depth of the reflectors will be based on the travel time. A study of the amplitudes of the pdP phases from each region will give the estimated contrasts of physical parameters at the proposed boundaries. After the establishment of a model for these reflectors, we shall investigate additional evidence which should help prove or disprove the existence of the model. We hope to find, at near stations, the P-SV converted waves due to the boundaries that give rise to pdP. WWSSN records of South American events will be used here. Gaps in deep seismicity trends and island arcs have been well defined and discussed by others. In Chapter IV we will discuss the correlation between the gaps and the reflecting layer and whether the pdP phase could be reflected from the

upper boundary of these gaps or from some other irregular region. The effect of scattering by inhomogeneities in the upper mantle will also be discussed at the end of this chapter. Finally we will make a conclusion about the reflectors and the observations of pdP phase.

Chapter II

Data Source and Analysis

As an example, figure 1 shows the twelve traces of the subarray sums of LASA from an earthquake with a focus placed in the Preliminary Determination of Epicenter (PDE) list at 537 km depth under northwest Argentina. The coherent precursors to pP are clearly shown. There are a few possible interpretations of these precursors to pP. PcP is the most commonly recognized phase between p and pP from beyond 50°; however in our study, we especially tried to avoid the misreading of the PcP phases. The precursors to pP could be interpreted as aftershocks of the main event. Although deep earthquakes usually do not trigger aftershocks, we can not rule this out unless we can find similar phases for deep events from the same region. We could also interpret the precursors as phases reflecting from the bottom of the crust beneath the stations. However, in this case, these phases should generally be observed independent of the geographic region or depth of the sources. Finally, the most probable alternative is that these phases are due to the reflection by upper mantle discontinuities. In the last section of this chapter we will extend this interpretation.

2.1 Data Source

To study the precursors of pP, we first need to observe a clear pP phase. For deep events, PCP arrives at the same

time as pP for epicentral distances between 35° and 55°, confusing the identification of pP precursors. Thus we have to use records of deep earthquakes from teleseismic stations as our data. Since, there are not many deep earthquakes with large magnitude, it has not been easy, as Adams (1968) pointed out, to study a very large number of pdP phases.

Fortunately, the establishment of seismic arrays has helped solve part of the problem. According to Davis (1973), an array system should satisfy the following criteria:

(1) Three or more sites at which seismometers are located.

(2) An aperture of more than one and less than a thousand kilometers.

(3) Uniform instrumentation and recording.

(4) Tape recording of individual channels.

(5) A vertical control point which will send out time signals to each site.

(6) A means of analysis of the data as an ensemble rather than in separate channels.

Thus from the digital recording of each channel we can use digital processing techniques to increase the signal-to-noise ratio, so as to make it easier for us to pick out the pdP phase. To understand the processing of our data, we would like to describe the fundamental characteristics of the sources of that data.

2.1.1 LASA arrays

The Large Aperture Seismic Array, LASA, began recording in 1964 in Eastern Montana. The array was built with a heavier concentration of seismometer at the center than on the flanks. It contains 525 short period vertical seismometers - which are grouped as shown in figure 2, into 21 subarrays. Each subarray also has at its center three orthogonal long period seismometers. The aperture of LASA is around 200 km. Operation of LASA is based on two fundamental principles; namely the suppression of noise and the directional discrimination capability of beams. The addition of each channel will decrease the random noise level and increase the coherent signal. However, before addition we should introduce suitable time delays. For scientific purposes, the aperture of each subarray is sufficiently small that the unphased sum of all its short-period seismometers is a very adequate representation of the signal. Thus in this thesis, we only use 21 subarray sums of data.

The digitalized records are fed to a central computer in Billings, Montana. From there, all data are dispatched by phone line to Washington, D.C. for immediate analysis. Around 20 kilo bits of seismic data are transmitted per second. The seismic data are stored on magnetic tape for further use.

We searched for all the deep events occurring between 1966 and 1973 at the LASA library in Lincoln Laboratory. As mentioned previously, earthquakes from five deep seismicity regions, South America, the Sea of Okhotsk, the Bonin Islands, the New Hebrides, and the Fiji-Tonga Islands were examined. Because of the poor capability of detection in the early period of installation, and tape errors, some deep and large earthquakes reported by the International Seismological Commission (ISC) were not investigated in this study. Other deep seismicity regions, like Mindanao, the Flores Sea, the Banda Sea, the Celebes Sea, and the Solomon Islands also have not been studied, because their epicentral distances were greater than 104° from LASA.

Table 1 lists the events in the five regions. The selected earthquakes in South America are mainly from three different areas, the Peru-Brazil border with a latitude of 9°S and longitude of 70°W, and the two Argentine provinces, Salta and Santiago Del Estero, having latitudes of 22°S and 27°S and the same longitude of 63°W. The epicentral distances from these areas are about 60°, 70°, and 80° respectively. Most earthquakes we used have a magnitude of greater than 5.0 and a depth of between 500 and 600 km. Twenty events from the Sea of Okhotsk, found in the LASA tapes library are shown in table 1. Only 5 events were deeper than 520 km, each of which occurred at about 50°N and 48°E. Other events

taken from scattered locations in the Sea of Okhotsk, south of Sakhlin Island, Kamchatka and eastern Russia, had depths of less than 520 km. The distance to LASA is around 77° to 57°.

We investigated 14 deep events recorded at LASA from the Bonin Islands region. Eight of these events occurred beneath the islands at a depth of between 438 and 578 km. Four events came from an area south of Honshu with a depth of less than 400 km. The remaining event was the deepest having a depth of 618 km and located beneath the Mariana Islands.

Very few deep earthquakes occurred at the New Hebrides region; however, in the Fiji-Tonga region, 32 events were used as shown in table 1. Since the average distance to LASA is 90° to 100°, we can hardly identify pdP phase from events with a magnitude of less than 5.0.

2.1.2 NORSAR

NORSAR, the Norwegian Space Seismic Array, was completed in 1971 just north of Oslo, Norway as a joint U.S.-Norwegian venture. Design concepts of NORSAR are similar to LASA (figure 3). The array aperture is uniformly filled, with a total diameter of around 100 km. There are 22 subarrays, each having 6 short period seismometers. At the center of each subarray three orthogonal long period seismometers were also installed.

In the reports of the evaluation of NORSAR, it is found that the short period amplitude scatter at NORSAR is larger than that at LASA. With the same distance and magnitude, LASA showed higher amplitudes than NORSAR. Frasier (1972) suggested that this might be because of the hard rock site under NORSAR. From our experience in observing NORSAR data, we also felt that signal-to-noise ratio at NORSAR was typically lower than for LASA events at the same distance. Also we observed more multiple reflections between P and pP at LASA.

We also used the NORSAR data in this study. However, data are available only from three regions: the Fiji-Tonga Islands, and the New Hebrides are too far from NORSAR leaving only two earthquakes from South America, five from the Sea of Okhotsk and five from the Bonin Island region available for study.

2.1.3 WWSSN

The World Wide Standard Seismic Network (WWSSN) made up of about 120 seismic stations over the world was installed in the early 1960's. Each station, using standard instruments, records both short and long period data on three components.

In order to increase the confidence of our observations, WWSSN records from three regions were also examined:

South America, the Sea of Okhotsk and the Bonin Islands. Again, in the Fiji-Tonga and Hebrides regions, because of the great epicentral distance from the stations with clear records, no good examples of pdP phases were found. Table 1 also lists the events we used in pdP search of WWSSN records. Only clean records with pdP phase were reported here. In Chapter III, we will also use some WWSSN records from nearby stations to examine the existence of these reflectors. We shall look for SV-P conversions at discontinuities implied by pdP reflections.

2.2 Methods of Analysis

Most of the labors of this study were spent in searching the precursors and identifying them. The methods include the beam-forming, $dT/d\Delta$ measurements and VESPA analysis. Before the explanation of these methods, we shall discuss the theory of seismic arrays. Like the analysis of the other signals, the wave sampling theory is grounded. However, seismic signals are transient and that leads to different approaches in signal processing. The waves will be characterized only by their angular frequency (w), horizontal wave number (k) and amplitude A(w,k). Descriptions of frequency wavenumber analysis have been given by Burg (1964), Capon (1969a) and Lacoss et al. (1969). For a certain field (signal or noise),

we can map the power p(k,f) as a function of wave number k, and frequency w. Assuming time and space are stationary, the power of the field is (where w = 2πF)

$$P(k_x,k_y f) = \iiint_{-\infty}^{\infty} R(\rho_x,\rho_y,\tau)\exp\{-2\pi i(f\tau+k_x\rho_x+k_y\rho_y)\}d\rho_x d\rho_y d\tau$$

where $R(\rho_x\rho_y\tau)$ is the auto-correlation of the field.

$$R(\rho_x\rho_y\tau) = E[\phi(x,y,\tau)\phi(x+\rho_x,y+\rho_y,t+\tau)]$$

means expectation and ϕ is the value of the field. This power can be determined either from the beam forming in the time or frequency domain (Lacoss et al. 1969).

2.2.1 Beam forming

One of the main purposes of the array system is to increase its capability of detection. Therefore we should maximize the improvement in signal-to-noise ratio while imposing a minimal distortion on the wave form of the arrival signal. Extensive investigation has been made using various methods by combining the individual sensor output from arrays. Four-array processing schemes have been discussed by Green et al. (1966) and Capon et al. (1967, 1968, 1969). The simplest one is the straight summation combining of the seismometer output. Although it decreases the noise level, the distortion of signal

makes it useless.

For delay-and-sum, referred to as DS processing, only a delay to align the signals is applied to each seismometer. The velocity determining the delay from seismometer to seismometer is usually determined from the signal characteristics at each seismometer. It will provide the maximum signal-to-noise ratio if all sensors have identical signal wave forms and have independent noise of equal powers. However, in the case of seismic waves, this is not true because the noises between sensors are correlated so that delay and sum are not optimum.

The next scheme, in order of complication, is the weighted delay and sum which attempt to modify the array pattern by applying amplitude coefficients to each element in addition to the steering delay. The most complicated of the four methods, filter-and-sum, establishes a delay and amplitude weight for each element at each resolvably different frequency by filtering each trace and summing the filter output.

The determination of amplitude weighting coefficient in the weight-and-sum process and the filter function in the filter-and-sum process could be approached by using the maximum-likelihood method. As a result, the improvement of the signal-to-noise ratio is proportional to the complexity of the processing. The last two processes,

although yielding greater improvements, require a considerable amount of processing time. This is not practical in our study. Moreover, since the frequency wave number spectrum of the microseismic noise has been found to have a diffuse structure in wave number space, (Capon, 1973), the signal-to-noise ratio gain obtained by delay-and-sum processing is almost the same as that of the filter-and-sum process.

The so-called "beamforming" is included in the first three of the four schemes. In our analysis, only the delay-and-sum technique is used. We could display the subarray sums of each channel on paper. For accuracy, we did not use the conventional method to find the delay by given apparent phase velocity, instead, we asligned the first 2 cycles of P waves by eye. After the time alignment of 21 channels, the traces are summed and the sum divided by 21. Enhancement of the coherent phases is expected. Figure 4 shows an example of this "beamforming" trace and the associate subarray traces of an event that occurred in the Sea of Okhotsk. We notice that the signal-to-noise ratio has improved compared to the subarray traces and a clearly intermediate phase between P and pP is revealed. In figure 5 we also show a few examples of beamed traces of earthquakes from other regions on which precursors to pP can be easily identified. However, this is not always

the case. Although we use the beamforming technique, beam traces of certain deep events do not show any clear or obvious phase between P and pP.

2.2.2 VESPA

As described at the beginning of this section, we can measure various seismic parameters at the array. The important parameters are the azimuth and the apparent phase velocity crossing the array. A convenient way to analyze velocity is in terms of energy as a function of time and velocity at the array. This process was first used by Davis, Kelly and Filson (1971), it is called Velocity Spectral Analysis or VESPA. Since each ray path has a constant ray parameter P or $dT/d\Delta$, it is more suitable to replace the velocity by the slowness or inverse phase velocity of signals. The process involves the formation of a beam by delay-and-sum over a specified time window which is stepped down the record. This is then repeated for different slownesses keeping the beam at a constant azimuth until a two-dimensional contour plot (vespagram) of power versus slowness and time is generated.

The beam width in azimuth is about 2°. Most compressional body wave signals (p wave) received at a seismic station have a $dT/d\Delta$ of between 12.0 sec/degree for close events and zero for events at the antipodes. Any signal with a $dT/d\Delta$ of less than 4.55/degree has either transversed

the earth's core or has been reflected from it. In the teleseismic zone from 30° to 90° $dT/d\Delta$ decreases fairly linearly from 9.0 to 4.5 sec/degree. Thus in a vespagram, we can look for the point in time and slowness where high energy is concentrated. From the knowledge of slowness and arrival time, we can understand the property of this signal. It enables us to separate signals which approach with different phase velocities but arrive at the same time from the same azimuth, even when signals are of comparable amplitude.

As an example, figure 6 shows the slowness response of LASA versus time for an earthquake with depth 630 km, which occurred on October 12, 1967 just west of the Tonga Islands. Power is contoured at 2 db intervals and the array was aimed in the epicentral azimuth. The beams have $dt/d\Delta$ values from 0 to 125 degree^{-1} in steps of 0.25 degree^{-1}. A few subarray traces are shown beneath the vespagram display with the same time scale. We can see the clear intermediate phase which arrives at about 60 sec before pP. It corresponds to the point where the energy is concentrated between P and pP.

The peak of the contour group is at a slightly greater slowness than the p phase and at a slightly lower slowness than the pP phase. This is generally found to be true according to our experience of the pdP study and is consistent with our interpretation of the phase originating

at a point shallower than the focus and closer to the array.

In our analysis, VESPA will be used as an auxiliary technique to examine those identifications of poor quality phases found on the beam. Next, we will discuss an additional method of verifying the origin of the pdP phases.

2.2.3 Location schemes

During the "beamforming" process, after the time alignment of P waves is made, the arrival time difference relative to the center of the array can be found. The fixed geographic location of each site is used to calculate the azimuth and the apparent phase velocity. We use a least squares method to find a plane wave which will give the best fit to those time differences found in the phase alignment. Through the use of a standard travel time curve, and its slope, the velocity and azimuth measurements may be converted to a source location.

Any unknown coherent phases in the subarray sums, if they are clear enough, may also be aligned by eye. The location schemes will consider it as a P wave and calculate its apparent velocity to examine whether it has P phase velocity and then report the epicenter, azimuth epicentral distance and apparent phase velocity. Of course, this does not represent the actual epicenter. We don't know the ray path of the coming plane wave. It might be a near event or a reflection from the crust or other boundary. Although we call this location the "equivalent epicenter", this scheme is useful in our determination of the source of the pre-

cursors.

In figure 7, assuming the ray paths are from the same azimuth, the equivalent epicentral distances of these precursors will be greater than those of pP and less than those of P. More clearly, we can express this as

$$\Delta(P) > \Delta(pdP) > \Delta(pP)$$

or

$$V(P) > V(pdP) > V(pP)$$

where Δ is the equivalent epicentral distance and V is the apparent phase velocity.

We applied this scheme to verious P, pdP and pP phases; the results are consistent with our interpretation. As an example, table 2 gives the calculated horizontal phase velocities and equivalent epicenters of Event 40. Although pdP and pP show lower root mean square error from the time alignment, the azimuths are fairly close. Apparent velocities and equivalent epicentral distance are decreasing in the order of p, pdP to pP, thus giving greater confidence in our hypothesis. The precise apparent phase velocities will allow us to estimate the dip angle of each phase which will be used in the amplitude study.

For low signal-to-noise ratio records, it is difficult to do the beamforming to those precursors; however, we can use station corrections and theoretical delays to form the beam for given slowness. It is found that some subarrays systematically show earlier or later arrival times than

theoretically expected. This might be due to the crustal structure beneath the array. Engdahl and Felix (1971) defined the "relative subarray travel time anomaly" as

$$A_{j/i} = (O_j - O_i) - (T_j - T_i) + H$$

where $A_{j/i}$ is the anomaly of the j^{th} subarray relative to the i^{th} subarray.

O is the observed arrival time of phase on subarray beam.

T is the theoretical arrival time of phase at the subarray centers.

H is the correlation for elevation difference between i^{th} and j^{th} subarray center elements.

The $A_{j/i}$'s are also known as "station connections" at LASA, and the reference subarray is taken as the center subarray A_o. It is the same reference site used in the beamforming. These station corrections are stored in the computer and also have been used in beamforming and location schemes to get more precise results.

2.3 Results and Characteristics of the Observation

The most commonly used array technique used in this study was beamforming. We reat the precursors and recorded the time interval between pdP and pP. All of the events were read independently, without reference to other earthquakes or a travel-time table, and all the readings were made by the author in an effort to be systematic.

The readings of the precursors were graded as good, fair and poor. The good quality readings are those with a sharp pulse or a wave train with a sharp beginning. The signal with an emergent beginning but a definite signal, will be considered fair, those small signals with an emergent beginning and hard to distinguish from the prevailing background noise will be graded as poor.

No correction for the earth's ellipticity was made. We reexamined those poor quality LASA data by VESPA analysis to make sure of the identification. A few of good quality LASA records from each region are used in the location scheme. We did not use station corrections and theoretical delays to beam the precursor because of the uncertainty in the slowness. None of these processes can be used on the WWSSN records. Tables 3 to 7 give the observational results of five regions. The precursor subscript depends on the time difference between pP, pd_1P designates those precursors arriving within 40 sec before pP, pd_2P those within 50 to 70 seconds. and pd_3P those with time differences greater than 70 seconds. The evaluation of the quality of the data is discussed here and certain amplitude ratios between P and pP are listed.

As a result of observation, we tend to reject the two possibilities of interpretation which were mentioned in the beginning of this chapter. We found similar precursors from different sources in each region. The slownesses of

these precursors are systematically higher than the P phase. This eliminates the suggestion of aftershocks because aftershocks would tend to occur in a scattered pattern around the main shock.

The possibility of interpreting these precursors as due to the reflecting layer beneath the array is also rejected because we cannot find any clear evidence of these precursors from shallow earthquakes or explosions. From the evidence of our analysis, we interpret these precursors as being the reflection phases from the discontinuities between the foci and the surface. Figures 8 through 11 plot the time interval between pdP and pP with respect to epicentral distance; in these plots the quality of data is represented by various symbols. Although different from place to place, we still can see the pP-pdP time differences are concentrated within a few time intervals.

The observation of these precursors was influenced by many factors, e.g. background noise at the station, character of the earthquake, and the contrasts of the physical parameters at the reflection point. From our observational experience, most of the good examples of pdP have a strong pP phase relative to P. However, some records violate this generality and suggest that either their ray paths vary considerably or that the reflection coefficient is just too small at the interface.

It is more difficult to identify the pdP precursors on

WWSSN records, but we still have considerable evidence from this source. Some examples are shown in figure 12. In searching for the precursors on WWSSN records, it is better to examine the shape of the signals and to compare the periods with P and pP. In general, it is found that the later arrivals will have a longer period on short period records. This is because the later arrivals will have traveled longer through the low Q region of the upper mantle than the initial P phase. Although "beamforming" can increase the signal-to-noise ratio, the slight difference in slowness between P and reflected phases will decrease the amplitudes of pdP and pP when we form the beam with respect to the P phase. pdP and pP on the beam trace show smaller amplitude than the subarray channels. Although this won't influence our identification much, it will be important in the amplitude study.

Chapter III

pdP phase and Upper Mantle Discontinuities

The term 'discontinuity' will refer to a sharp variation of seismic velocity with depth. This may be a discontinuous velocity jump (a first order discontinuity) such as the Mohorovičić discontinuity or a continuous velocity structure that is discontinuous in one of the derivatives of velocity with respect to depth (the second order or higher order discontinuity). A chemically homogeneous planet with no solid-solid or solid-liquid phase changes will have a smoothly varying velocity curve. Thus 'discontinuities' in the velocity-depth curves in the earth's mantle would also represent departures from homogeneity as defined above.

In the upper mantle, four possible discontinuities have been suggested from body wave precursors and surface wave studies as stated in the previous review. Our only interest is the region above deep earthquake sources. To characterize the discontinuities we shall attempt to determine their depth and the associated contrasts of physical parameters.

3.1 Depth Estimation from Travel Time

In PdP and P'dP' studies, workers estimate the depth of the discontinuity simply by reading the half value of the time interval between precursors and main phase. However,

since the deep phases are not symmetrical our estimation will be from a different basis.

Considering a homogeneous upper mantle, the ray paths of pP and pdP should be very close, especially before reflection. Thus the travel time difference between pP and pdP of a deep earthquake is approximately equal to the time interval between pP and P of an event occurring at the reflector with depth d. Figure 13 shows the ray paths from a simple flat two layer model and a homogeneous earth model. From the pP-P time table in the Seismological Table for P phases by Bolt et al. (1968), we can estimate the depth of the reflector (d) by reading the time interval between pP and the observed pdP for given distance. Thus, for each reading of precursor in table 3 to 7, we estimated the depth independently following the above method and plot it with respect to the epicentral distance with different symbols to represent our confidence in the reading. We shall discuss these results region by region.

In South America, deep earthquakes mainly occurred in the following regions; west Brazil and Peru Border, Salta province, and Santiago Del Estero province of Argentina with average distances to LASA, 65°, 78° and 83° degrees respectively. The azimuth range of these sources with respect to LASA is 329° to 332°. Figure 14 shows the estimated depths of the relfector in this area. There are four clearly separated

intervals, from 100 to 140 km, 240 to 260 km, 280 to 390 km and from 360 to 400 km. Three different earthquake provinces show different reflectors. If our hypothesis is correct, it will suggest four reflection regions beneath the Brazil and Peru Border, two beneath Salta province and three beneath Santiago province. For convenience, we will interpret these four discontinuities from their center depth, i.e. at 120, 250, 280 and 380 km. (Two NORSAR reports of events 12 and 13 show slightly lower estimations than from WWSSN data.) Event 11 doesn't belong to any of the three mentioned regions, but the estimated reflection depths are within the range of our other estimated depths. To determine whether all four reflection zones exist in all three provinces, we examine the vespagrams. For event 9, with poor quality in our interpretation, we found: at 32 sec. before pP, there is a signal (12db) with slowness 5.5 deg/sec., and at 57 sec. before pP there is a signal (14db) with slowness 5.58 deg/sec. Both are reported in our analysis. However there are few more closed contours with correct slowness at 69 and 65 seconds before pP. According to our interpretation they will correspond to discontinuities at 300 and 275 km. We leave out the one arriving 65 seconds before pP because it has the same slowness as p.

The deep earthquakes in our second region occurred beneath the Sea of Okhotsk and East Russian Border. The

later has a more complicated upper mantle because it is located at the intersection of three island arcs. Complexity in the estimation of the depth of the reflectors is expected. However, figure 15 does not show this. From three good records of this area, we estimate the depths of the reflectors to be 80, 130, 230, 270 and 350 km. We suggest that there are three major discontinuity regions with depths of between 80 to 140, 220 to 290 and 320 to 400 km. Comparing the discontinuity regions with those of South America, the two upper discontinuities seem to extend to more shallow regions and no good reflectors are found between 280 and 320 km. Furthermore there is no gap from 260 to 280 km. Events 22, 27 and 31 are located at 50°N, 147.5°E with a depth of greater than 550 km; their records at LASA and WWSSN stations consistently gave estimation of reflection depths to be 380 to 390 km which other events do not show. This is because in the case of shallow earthquakes, the precursors are too close to the main P phase to be able to distinguish them from P wave codas and pcP at this distance. Events 28 and 29 give a greater estimation of the depth of the second discontinuities. However, event 19, which occurred at the same region didn't show this reflector.

Within the Bonin Islands region, event 40 is from the Sea of Japan and event 46 occurred beneath the Mariana Islands. Other events are distributed around Southern Honshu

and the Bonin Islands. The depth versus distance plot of the reflection (figure 16) apparently shows different configuration than in the two previous regions. There is a strong reflector at about 160-200 km depth in this region. Above that, the reflection range within the low velocity zone seems narrower and the three identifications at 75-80 km are made with less confidence. Between the range of 230-400 km, the 230-270 km and 300-320 km zones can be easily identified by a high density of readings and adjoining zones of few or no data points. Only a few earthquakes deeper than 500 km give good results below 350 km, such as events 37, 39, 46, and 47. No significant difference exists between the two mentioned special regions, except event 46 gives a reflection at 280 km, which is a low quality reading.

In the Fiji-Tonga region, only LASA data are available. Deep earthquakes in this region have an average distance to LASA of greater than 89°. Precursors to pP are comparatively smaller in amplitude. Despite this, we tend to interpret the depth of the reflections into 5 regions as shown in figure 17. The uppermost discontinuity, as narrow as that in the Bonin Islands, is from 110 to 140 km. Again there is an indication of some arrivals from 160 to 180 km, but no good quality reflectors were found here. The other three regions are 210-260 km, 280-300 km and 330-400 km. Although most events don't show phases from every reflector, it seems

these reflectors are fairly consistent throughout the region. For example, we have shown the vespagram of event 63 recorded at LASA in figure 6. At about the same slowness there are two peak contours of 22 dB at 40 and 85 seconds before pP, and two 24 dB counters at 74 and 64 seconds before pP. According to our hypothesis, these will correspond to discontinuities at 170, 225, 320 and 370 km. These are not clear enough to identify on the array beams because of their small amplitude. Event 67 is located north of the Kermediac Islands and 100.6° from LASA. We found three reflectors at depths of 105, 210 and 280 km on the LASA recordings of this event. The triangle symbols in figure 17 represent the events 53 and 54 from the New Hebrides. Reflectors were estimated with depths of 235, 250, 260, 300, 375 and 400 km; no reflectors shallower than 235 km were found.

To summarize, we found reflectors within the low velocity zone centered at 110-120 km with a width of 30 to 60 km in all regions studied. However, beneath the Fiji-Tonga and Bonin Islands, this region narrows to 30 km. Precursors occurring at 20 sec and 30 sec before pP are probably reflected from the top (80 km) and the bottom of a low velocity zone. These zones were predicted to exhibit very sharp changes in velocity. Reflections between 160 and 200 km only exist in the Fiji-Tonga and Bonin Islands region. This interpretation is consistent with the results of Adam's

(1968). Between 200 and 400 km, reflectors appeared mainly at depths of between 230 and 320 km. Three areas show a 20-30 km gap with different lower and upper bounds, but in the Sea of Okhotsk region reflectors exist from 230-280 km. Shallower events in the Bonin Islands and in South America, have very few reflectors below 320 km, but beneath the Sea of Okhotsk and Fiji-Tonga regions, the reflectors are found below that depth.

3.2 Characteristics of Discontinuity From Amplitude Study

For a two solid semi-infinite elastic media with a different character, an incident p wave at the plane interface will generally produce compressional and distortional waves in both media. Four boundary conditions must be satisfied, requiring continuity of the two components of displacement and two stresses across the interface. Following the notation given Ewing Jardetsky and Press (1957) as given in figure 18, we will use subscripts 1 and 2 to refer to the incident and reflected waves respectfully, and accents to refer to the transmitted waves. Let ϕ and ψ be the p and s wave potential functions, then for an incident P wave we have

$$\phi = A_1 \exp[ik(ct-x+az)] + A_2 \exp[ik(ct-x-az)]$$

$$\psi = B_2 \exp[ik(ct-x-bz)]$$

$$\phi' = A'\exp[ik(ct-x+a'z)]$$

$$\psi' = B'\exp[ik(ct-x+b'z)]$$

where a = tan e, b = tan f, a' = tan e' b' = tan f' and c is the apparent velocity across the interface.

By applying the four boundary conditions, which in our notation will be u = u', w = w', $p_{zz} = p_{zz}'$, $p_{zx} = p'_{zx}$ at z = 0, we get

$$A_1+A_2-bBa = A'+b'B'$$

$$a(A_1-A_2)-B = a'A'-B'$$

$$\rho\beta^2\{-(b^2-1)(A_1+A_2)-2bB_z\} = \rho'\beta'^2\{-(b'^2-1)A'+2b'B'\}$$

$$\rho\beta^2\{2a(A_1-A_2)+(b^2-1)B_z\} = \rho'\beta'^2\{2a'A'+(b'^2-1)B'\}$$

Thus, solving the four equations, the p wave reflection coefficients will be

$$A_2/A_1 = \frac{(l_1-l_3)(m_2+m_4)-(l_2+l_4)(m_1-m_3)}{(l_1+l_3)(m_2+m_4)-(l_2+l_4)(m_1+m_3)}$$

and transmission coefficient

$$A'/A_1 = \frac{2(m_2+m_4)}{(l_1+l_3)(m_2+m_4)-(l_2+l_4)(m_1+m_3)}$$

where

$$l_1 = \frac{2\mu+\mu'(b'^2-1)}{\mu(b^2+1)} \qquad m_1 = \frac{2b'(\mu-\mu')}{\mu(b^2+1)}$$

$$l_2 = \frac{\mu(b^2-1)-\mu'(b'^2-1)}{\mu b(b^2+1)} \qquad m_2 = \frac{b'[2\mu'+\mu(b^2-1)]}{\mu b(b^2+1)}$$

$$l_3 = \frac{a'[2\mu'+\mu(b^2-1)]}{\mu a(b^2+1)} \qquad m_3 = \frac{\mu(b^2-1)-\mu'(b'^2-1)}{\mu a(b^2+1)}$$

$$l_4 = \frac{2a'(\mu-\mu')}{\mu b(b^2+1)} \qquad m_4 = \frac{2\mu+\mu'(b'^2-1)}{\mu(b^2+1)}$$

To estimate, in our case, the physical parameters from observational results using the calculated reflection and transmission coefficients would be too complicated. Gutenberg (1912) gave only curves for the square root of the energy ratio of the reflected and transmitted waves for several models. These do not help in our inversion. We shall use more general results by McCamy et al. (1962). Although some error in their paper has been pointed out by

Singh et al. (1970) and Hale and Roberts (1974), these errors do not affect the transmission and reflection coefficients for incident p-waves.

We proposed four reflectors in the preceding section, two of them have been discussed by others, the known low velocity zone between 80 and 160 km, and the '20° degree discontinuities' where olivine changes to spinel structure between 360 and 410 km. However, because of the uncertainty about the characteristics of these two reflectors, it will be irrelevant to estimate the physical character of the other two reflectors from a four layered model directly. We can only estimate contracts layer by layer. We measured the amplitude ratio of pP to P and of pdP to pP separately as listed in tables 3-7. As mentioned previously, the amplitude of pdP and pP on the beam traces are smaller than those on the subarray traces owing to the fact that we used p wave slowness in beamforming which was slightly different from those of pdP and pP. In our measurements we took the average amplitude pP and pdP on subarray sums of array data. For WWSSN records, we simply measured the amplitude.

Since ray paths of the p wave are much different from those of pdP and pP, the energy carried by the p waves before reflection is related to the radiation pattern. Thus the amplitude ratio of pP to P will be useless in the estimation of physical contrasts at the reflectors. However

it will give some feeling about the quality and confidence of the interpretation of the precursors. Only the amplitude ratio of pdP to pP will be used in the following study.

First of all, we shall find the velocity change of the topmost reflector by investigating a few high quality precursors. For example, Event 2 of the South America region has a good precursor recording at 27.5 sec before pP at LASA. The estimated depth of the reflector is 120 km. The ray path of this precursor is different from pP phase only after it is reflected at 120 km (figure 19). With the same notations for normal incidence,

$$A_2"/A_2 = (\rho_2\alpha_2-\rho_1\alpha_1)/(\rho_1\alpha_1+\rho_2\alpha_2)$$

$$A_1/A_2 = 2\rho_1\alpha_1/(\rho_1\alpha_1+\rho_2\alpha_2)$$

$$A_1' = -A_1 \qquad A_2'/A_1' = 2\rho_2\alpha_2/(\rho_1\alpha_1+\rho_2\alpha_2)$$

or $$A_2'/A_2 = \frac{-4\rho_1\alpha_1\rho_2\alpha_2}{(\rho_1\alpha_1+\rho_2\alpha_2)^2}$$

then $$A_1"/A_2' = \frac{1}{4}\left[\frac{\rho_2\alpha_2}{\rho_1\alpha_1} - \frac{\rho_1\alpha_1}{\rho_2\alpha_2}\right] \qquad (1)$$

Thus, for a given ratio of $A_2"/A_2'$ we can find the impedance ratio.

The measured ratio of pdP to pP does not equal $A_2"/A_2'$. Two factors are responsible for this. First, the reflection coefficients are a function of incidence angle. Unlike the p'p' precursor study, the incidence angles of pdP and pP at

the reflectors are between 25° and 15°; we can't neglect this influence. Second, although the remaining ray paths of pdP and pP are the same, both refract at other boundaries and pass once through the low velocity zone beneath the station. The pP waves will have a much higher attenuation than pdP, because they travel twice as fast in the low Q zone before being refracted at the inner side of the discontinuity. These two effects should be normalized before we use formula (1).

Our measurement in event 2 shows that $A_2"/A_2'$ is 0.25. If we designate the inner side of the 120 km reflector as having a p wave velocity of 8 km/sec, the incidence angles of pdP and pP are 21° and 23° respectively. From the plots by McCarry (1962), using a 21° incidence angle, we find that the reflection coefficient will decrease about 15 per cent systematically from its maximum value (normal incidence; if the impedance ratio is within 1.8 to 1.2. But there is no significant change in transmission coefficient (after Gutenberg). To estimate the attenuation, we select the average Q to be 90, pP travels 200 km within the low Q zone, and the average p wave having velocity of 7.5 kn/sec. The attenuation of the signal with 1 second period will be $e^{-0.93}$. In other words the normalized pP at the inner side of the discontinuity will be 2.54 times the measured value. The reflection coefficient will be 0.85 at the surface (after Gutenberg). Together with the first effect, the

normalized amplitude ratio should be $A_2"/2.54A_2'$ or 39 per cent of the measured ratio. Substituting the normalized ratio for formula (1) we have

$$\frac{\rho_2\alpha_2}{\rho_1\alpha_1} = 1.30$$

Using Birch's relation between p wave velocities and density

$$\rho = 0.328\alpha + 0.768$$

and α_2 = 8 km/sec ρ_2 = 3.39 g/cc, we get α_1 = 6.9 km/sec which is a very low velocity compared to other models. It might be the effects of source mechanism or some particular feature on the ray path of pP which gives it a comparatively low amplitude.

For other events of South America, the amplitude ratios of pdP to pP are between 0.15 to 0.2. Following the above arguments it will have a p wave velocity of 7 - 7.25 km/sec above the reflector which is still lower than most models. Whitcomb (1972) in his p'p' precursors study suggests that a dipping, reflecting interface will cause residuals in arrival time. In our case, pdP could be reflected at the boundary of the downgoing slab, with an incidence angle of greater than 50°. The reflection coefficient will only decrease 40%, however, the transmitted energy will decrease to zero in the vicinity of 60°. This might be the reason that we observed a higher amplitude ratio.

The estimated second reflectors are 250 km deep in the

Salta province, and 270 km deep in the Santiago del Estero province and Brazil-Peru border region. The measured amplitude ratios of these pdP phases are 0.35 and 0.2 respectively. For horizontal interface, the incidence angle of the ray path to LASA will be 25° from Salta, 23° from Santiago and 28° from the Brazil-Peru border. Following the preceeding arguments, the transmission coefficients at the 120 km reflector with a 10 percent velocity change are about 0.9 for upgoing waves and 0.8 for downgoing waves. Thus the amplitude ratio of pdP to pP will be

$$\frac{A_3''}{A_3} = 0.347 \left(\frac{\alpha_3\rho_3}{\alpha_2\rho_2} - \frac{\alpha_2\rho_2}{\alpha_3\rho_3}\right)$$

The calculated impedance ratio at 250 km in Salta is 1.29, and 1.18 at 270 km for the other two regions. Assuming p wave velocity, α_3 is 8.5 km/sec. We will get 7.36 and 7.75 km/sec above 250 and 270 km respectively. The latter corresponds to a 9% change in velocity which is consistent with the results of Whitcomb and Anderson (1970). At 280 km discontinuity from P'P' precursor, using WWSSN records at Bulawayo (BUL) of event 8, the P wave velocity contrast will correspond to a 15% change which is much higher than other cases.

In the Sea of Okhotsk region, we chose LASA records of Event 15 to investigate the velocity contrasts. Three estimated reflectors at depts of 80, 265 and 354 km have corresponding amplitude ratios of 0.25, 0.25 and 0.4 on

the beam traces. We normalized the amplitude ratio of pdP/pP to 0.06, according to the incidence angle at the reflection point and the attenuation of pP phase in the low velocity zone; the resulting impedance contrast is 1.203. According to Birch's density and velocity relation, it will correspond to a 10% change in velocity and an 8% change in density; again this is higher than most models. To find the impedance contrast of the second reflector, the energy loss of pP which refracted at the first layer is also counted in the normalization of the amplitude ratio. For an 8.5 km/sec p wave velocity at the innerside of the discontinuity, we get 8% change in velocity and 7% change in density. The calculated impedance contrast of the third reflector at 354 is 1.22 after the normalization of the amplitude ratio. The velocity of p wave, 'α_2', will be 8.5 km/sec if we assume a 9.5 km/sec velocity on the inner side of the third interface; therefore suggesting a 105% velocity change and a 8.6% change in density.

Following the same procedure, we investigated the velocity change between the interface, from good LASA records of events 39 and 40 in the Bonin Islands region, event 53 in the New Hebrides and events 82 and 63 in the Fiji-Tonga region. We list our results in table 8. As pointed out in the last section, both the Bonin Islands and the Fiji-Tonga have a reflection region of between 160 and 200 km. The results of our calculation show this region

has a comparatively lower velocity change than in other discontinuities. For some deep earthquakes, for example, event 63, we found a strong signal of about 6 dB lower than the P wave peak which arrived 111 seconds before pP. This is probably the reflection phase from the 650 km discontinuities, because its slowness is slightly less than the main P phase. However, from our estimation based on the amplitude ratio, the velocity change will be higher than Ringwood (1970) suggests.

In general, our calculation shows higher velocity change in low velocity zone. Beneath the Fiji-Tonga and Bonin Islands regions between 160 to 200 km has 5 to 6.5 percent velocity change. While in other reflection regions at depths of 230 — 260 km, 280 - 320 km and 350 - 400 km, an 8 to 10 percent velocity change is shown on the average. A few results out of this range might be caused by anomalous structures within the upper mantle.

The primary chemical composition of the upper mantle corresponds to a mixture of about 3 parts of peridotite to 1 part basalt. This composition is termed pyrolite. Throughout most parts of the upper mantle, material of pyrolite composition would crystalize to a mineral assemblage composed of olivine, pyroxenes, and garnet. In the low velocity zone a number of phase changes have been proposed above 100 km. Whitcomb and Anderson (1970) list a few candidates, such as

$$3MgSiO_3 \cdot xAl_2O_3 = xMg_3Al_2Si_3O_{12} + 3(1-x)MgSiO_3$$

Alternatively, Anderson and Sammis (1969) suggest that the low velocity zone is due to partial melting. If this is true, the top and bottom of the low velocity zone should be good reflectors because of the large velocity decrease associated with the presence of a small amount of melt. Our result tends to confirm this explanation, but we shouldn't forget that the earthquakes we studied all occurred at deep seismicity regions. The precursors may be associated with the boundary of the downgoing slab.

Below 150 km and extending to 350 km, according to Ringwood (1970), the upper mantle appears to be homogeneous and phase transformation of pyrolite to denser structure has not been discovered in the relevant p-T range. However, Whitcomb and Anderson (1970) interpret the 280 km discontinuity as the onset of solid solution of pyroxene into garnet. Thus the precursors which are suggested as reflection at the boundaries between 160 and 200 km underneath Fiji-Tonga and Bonin Islands could come from two possible origins. Either they are reflected at the lower boundary of the low velocity zone which extends to the vicinity of 180 km or they are reflected at the boundary of the slab. We have strong evidence from WWSSN records at different azimuths for the reflectors between 230 to 260 km and 280 to 320 km. It is irrelevant to consider them as reflected from the boundary of the slab.

In the range from 350 to 420 km, experiemntal investigations show this continuity is almost certainly caused by two major phase transformations; the olivine-spinel-beta Mg_2SiO_4 transformation and the pyroxene-garnet transformation. Ringwood and Major (1970) discovered that magnesium-rich olivine transforms at high pressure to a distorted olivine-like structure, β spinel, with a density increase of about 7.5% instead of a true spinel structure, which is 10% denser than olivine. The details of the phase diagram of the system Mg_2SiO_4-Fe_2SiO_4 are uncertain at the high pressure forsterite end, but it is probable that the β spinel transforms to a true spinel system at higher pressure. With the temperature of 1600°C at 400 km deep and 30 bars/°C of gradients dP/dT at phase boundary, it will have the effect of increasing the pressure by 18 Kb and the median pressure for the transition would be 132 Kb. Thus the transformation of olivine through spinel into β phase would have occurred at a median depth of 397 km with a width of about 27 km.

The pyroxene-garnet transformation was also discovered by Ringwood (1967). He found that pyroxene will form extensive solid solutions with garnet at pressures on the order of 100 kb at 1000°C. If the mantle contains 8-10% Al_2O_3, the entire pyroxene component of the mantle can be transformed to the garnet structure and this will proceed to completion slightly before the onset of the olivine-spinel or olivine-β spinel transformation. This transformation is accompanied

by an effective increase in density of the pyroxene component by about 10% and it may be expected to occur at lesser depths than the previous transformation.

The amplitude and periods of reflection can give quantitative information on the sharpness of the reflecting zones. However, the problem is complicated by the lack of information on shallow velocity structure at the reflecting site and the amplitude of the P phase before it is reflected. We feel, although pdP amplitude can be used to study the impedance difference, and it will give us some feeling about the contrasts, but since pP traveled further in the low velocity zone, it is difficult to normalize the attenuation and lateral variation effect correctly with respect to the amplitude of pP. Besides, in our experience, focal mechanisms will yield different amplitudes along each ray path. This leads to amplitude ratios of pdP to pP greater than 1.

3.3 Refracted P phase converted at discontinuity from SV source

Looking for more evidence about the discontinuities, we try here to use another approach. To avoid the difficulty caused by lateral heterogeneity and attenuation at the low velocity zone, it is better to consider using the deep earthquake records of near source stations. If there are discontinuities with significant impedance change above

the source, we should find the refracted P and S phases at those interfaces from P and SV source. The two phases with no conversion at the interfaces can be easily recognized on the seismogram, but these do not help in our analysis. The S phase converted from P at interfaces which arrives just before the main S phase will have lower amplitude in general. That leaves us to study the converted P observed at the surface from the incident S wave at the proposed upper mantle interface.

In the first section of this chapter, we derived the transmission and reflection coefficients of P waves at the interface from an incident P wave. With the same notation and boundary condition, if we substitute the incidence wave from P to SV, we will have

$$A_2+b(B_1-B_2) = A'+b'B'$$

$$-aA_2-B_1-B_2 = a'A'-B'$$

$$\rho\beta^2\{-(b^2-1)A_2+2b(B_1-B_2)\} = \rho'\beta'^2\{-(b'^2-1)A'+2b'B'\}$$

$$\rho\beta^2\{-2aA_2-(b^2-1)(B_1+B_2)\} = \rho'\beta'^2\{2a'A'+(b'^2-1)B'\}$$

and the transmission coefficient of the refracted P will be

$$\frac{A'}{B_1} = \frac{2(m_1+m_3)}{(l_1+l_3)(m_2+m_4)-(l_2+l_4)(m_1+m_3)}$$

where l_i's and m_i's are the same as those in section one.

Again, it is difficult to estimate the change of

physical parameters; however, this ratio can be attempted from the energy equations with the assumption of $\lambda = \mu$, $\sigma = 1/2$. The transmitted p wave will have an energy ratio of $\frac{\rho' \tan e'A'^2}{\rho \tan fB_1^2}$ to the incidence SV waves. Gutenberg (1912) plots the square root of this ratio versus incidence angle. He indicates the maximum value of this ratio, 0.4, will occur at around 40° of incidence angle.

To simplify our problem, we consider the model with only two interfaces above the source. Amont all the conversion phases from this model two phases will comparatively have larger amplitude. The first one is the phase which has been converted to P from SV at the lower interface and undergoes no conversion afterwards. The second one is the phase which transmitted as SV at the lower interface and then converted to p at upper interface.

In South America, there are three WWSSN stations close to the deep seismicity zone. Thus we try to examine records of those events which were used in our pdP study. At Arequipa (ARE) Peru, the WWSSN short period vertical seismometer recorded a clear phase which arrived midway in time between the main P and S phases (figure 20). This earthquake is located in Santiago Del Estero province with a depth of 563 km which is event 14 in table 1. The epicentral distance to ARE is 13.5°. According to our interpretation, there are only two dominant discontinuities underneath this province which are centered at 120 and 280 km

and the estimated reflectors from LASA beam of this event are at 110 and 280 km. Assuming this phase is P phase which converted at 110 km from SV and with maximum energy, then the conversion will occur at about 3.5° away from the source in horizontal distance. The travel time after conversion could be found from the P wave travel time table by assuming that a 110 km event occurred at a distance of 10°. This time is 139 seconds. The travel time of S wave before conversion in our model is around 110 seconds. Thus this phase theoretically should arrive about 250 seconds after the onset wo it is consistent with our observation. Although there is not any information about the slowness of this phase, we tend to interpret it as a converted P phase at 110 km from the SV source. To consider this as a conversion phase from 280 km interface, it should theoretically arrive 225 seconds after the first motion. However, we do not find any apparent phase arriving at that time.

The amplitude ratio of this phase to s wave is about 0.1. Using Gutenberg's (1912) curves of the square root of energy ratio and our impedance contrast results from the last section, we find that the observation is low compared to the theory. This may indicate that our previous estimate of the impedance contrast at these depths is high.

Correlation Between Seismicity Gap and Reflecting Layer

Gaps in deep seismicity trends have been well described by others, but the origin and character are still open questions. Isacks and Molnar (1971), arguing from the point of view of stresses within the lithosphere, purposed two possible explanations for the gaps in seismic activity as a function of depth. One of them is that the lithosphere is considered continuous but the deviatroic stress goes to zero in changing from compression to extension. Alternatively, others suggest that the lithosphere is discontinuous, and that the gap in seismicity corresponds to a physical change in the lithosphere. Observations of the frequencies and amplitudes of seismic shear waves from deep earthquakes recorded at suitable locations might indicate the presence or absence of a discontinuous downgoing lithosphere. Evidence in the New Hebrides and Chile (Molnar and Oliver, 1969) of shear waves passing through the gap have been found. Further, the seismicity activity also indicates that in South America and the New Hebrides, pieces of lithosphere may be detached from the upper part.

To demonstrate this, we plot the seismicity activity versus depth in the dive regions which we are interested in. In Chile and Argentina, Peru and west Brazil, the cross sections are taken parallel to the plane which connect the latitude on surface and earth center. In other regions,

these planes are selected perpendicular to the trend of island arcs of: N45°E in the Sea of Okhotsk, N20°W in the New Hebrides, N25°W in the Bonin Islands, and N15°E in Fiji-Tonga region. The focal depth and epicenters are from the reports of USCGS between 1961-1970. We project geographic latitude and longitude of epicenters to the new coordinates and normalize them to represent its real length. In figure 21 a, we show the seismicity activity between 61° - 72°W and 21° - 28°S of 711 events in Chile and Argentina. The slab-like zone dip steeply at about 30° - 45° and reach a depth of about 300 km. Underneath theis, there is a pronounced gap between 300 and 500 km with only one event occurring at 350 km. At depths of 500-580 km, the earthquakes are active again and their hypocenters are confined to 2 narrow belts dipping more steeply to 50°. A similar configuration is shown in figure 21 b, however the slab-like zone of intermediate depth hypocenters, separated from a zone of shallow and probably crustal earthquakes that lies above it, has a dip angle of 10° - 15° and reaches a depth of about 200 km. The gap below 200 km extends deeper from 270 - 550 km and the separate lithosphere seems to go deeper to 660 km. This is in Peru and west Brazil, where there are fewer earthquakes. Only 372 events from 70° to 83°W and 6° to 11°S are present in this plot.

There is a seismicity in the New Hebrides region, a

gap. We only show 790 events within an area of 350 by 900 km which contain the deep earthquakes. We find the inclined seismic zone is very active at intermediate depths and the slab-like structure has a dep of about 75° - 80°. The evidence of a gap in activity between 290 and 580 km is very clear, but beneath 580 km, the hypocenters with depth predominantly between 580 and 660 km occur in a nearly horizontal, plane zone that in a map view is elliptical. Figure 21 d shows the frequency of earthquakes as a function of depth in the Sea of Okhotsk region. No earthquakes underneath the East Russia border are used and the few events with a depth of about 550 - 620 km are located at the south end of Sakhalin Island. We selected 951 events with a magnitude greater than 4.3 between 1960 and 1970. The gap between 230 and 350 km is still seen, but 3 events occurred within it. With a dip angle of about 45° - to°, the slab extends to 450 km, and then dips more steeply at 75° - 80° to 630 km.

The seismicity activity in the Southern Honhsu - Bonin Islands region (Fig. 21 e), and the Central Tonga (Fig. 21 f) does not show clear gaps as the above regions, although there is a lessening of activity density of occurrence in the center. The earthquakes we used here are 993 events between 27°W and 34°N, in Bonin Islands and 883 events within the area of 173° - 180°W and 19° - 23°S in Central Tonga.

In the last chapter we suggest an interpretation of the origin of precursors to consider that they are reflected from the boundaries of the slab; but some properties like velocity contrast, direction of ray path and depth of reflector should satisy this hypothesis. This sum doesn't fit our results. According to the model of Sleep (1972), the P wave velocity within the descending lithosphere is about 8 - 10% higher than in the outside area, which is counter to our conclusions from the amplitude study. In the Sea of Okhotsk, the ray paths of deep earthquakes to LASA are parallel to the trend of island arcs. Reflection can only occur at the upper boundary near the bottom of the slab. In the New Hebrides, the ray path of deep earthquake (>500 km) to LASA is away from the slab. Clear evidence of precursors of South American earthquakes are found from the WWSSN station in South Africa and Europe. All these seem to disagree with the slab reflection interpretation.

The boundaries of the seismicity gaps in some regions do show a slight correlation with the depth of the reflectors. Although using the same argument, the precursors cannot always be recognized as reflected at the gap boundaries. This correlation does suggest the possibility that the lithosphere below the gaps is detached from the upper part. We feel, the discontinuities within 230 to 350 km underneath island arcs are related to the character of the seismicity

gap and this will, at least, extend to a few hundred kilometers in horizontal. For detailed study we need a well-defined model and ray tracing technique to examine the reflecting point.

It has been argued that the coda waves of p are due to the scattering effect along the ray path. For teleseismic records of deep events, if there are scattered waves near the hypocenters, their arrival time will be very close to those of main p waves and their amplitude will be comparatively small because scattering is due to only very small change in physical parameters. The same argument could be used for those scattered waves in the center part of the ray path. We have tried to avoid those in data selection. Scattering of p waves under LASA, as Aki (1973) and Capon (1974) point out, could be very severe, however. Slowness will be greatly different from thos observed for pdPh. In general, we feel that although the scattered wave could exist, these precursors are not scattered waves.

Chapter V

Conclusions

The conclusions of the study are summarized as follows:

1. There is strong evidence, from VESPA analysis and slowness studies that observed precursors to pP are due to the body waves reflecting at discontinuities above deep earthquake sources. These precursors are neither waves scattered near the source nor waves scattered beneath the station.

2. An analysis of the travel time difference between precursors and pP phases of 87 deep earthquakes in five deep seismicity regions suggests that there are a few nearly horizontal reflectors within the upper mantle. They range as follows:

South America:	100 to 140 km, 240 to 260 km, 280 to 320 km and 340 to 400 km.
Sea of Okhotsk:	80 to 140 km, 220 to 290 km, 320 to 400 km.
Bonin Islands:	100 to 130 km, 160 to 200 km, 230 to 260 km, 300 to 330 km and 350 to 400 km.
Fiji-Tonga Islands:	110 to 140 km, 160 to 180 km, 230 to 260 km, 280 to 310 km and 330 to 400 km.
New Hebrides:	235 to 260 km, 300 km and 375 to 400 km.

3. The amplitude ratio study shows a larger velocity change in the low velocity zone that might be caused by the improper estimation of the normalization factor due to the path of pP in the low velocity zone. The estimated velocity change at other reflectors is 8-10% on the average which is in agreement with the results of Whitcomb and Anderson (1970). This velocity change suggests there is a phase change from olivine through spinel to β Mg_2SiO_4 between 350 and 400 km. The discontinuities between 230 to 300 km could be the onset of the solid solution of pyroxene into garnet. The two suggested discontinuities between 160 to 200 km, underneath Fiji-Tonga and Bonin Islands, with slight velocity changes, are not found elsewhere.

4. Another study was made of waves found at the near station which were converted at discontinuities to P waves from SV sources. The arrival time of the converted phase shows that it is refracted at the lower boundary of the low velocity zone. An amplitude study indicates a slightly lower velocity change at this boundary than was indicated by the pdP study.

5. In certain regions of deep earthquake sources considered in this study there are noticeable gaps in the seismicity depth profiles. Beneath South America, the New Hebrides, and the Sea of Okhotsk the boundaries of these gaps seem to correlate with the implied depths of the pdP phases.

TABLE 1

LISTS OF EARTHQUAKES DATA AND SOURCES

Event No.	Date	Origin Time h. m. s.	Lat	Lon	Depth km	Mag	Source L=LASA N=NORSAR W=WWSSN
		Region 1 South America					
1	Dec 20 1966	12 26 54.6	26.1S	63.2W	586	5.7	L
2	Jan 17 1967	01 07 54.3	27.4	63.3	588	5.6	W,L
3	Feb 15 1967	16 11 11.5	9.0	71.4	595	6.1	W
4	Sep 9 1967	10 06 44.1	27.7	63.1	578	5.8	L
5	Jan 31 1968	02 03 28.4	27.7	63.2	580	4.9	L
6	May 8 1968	04 20 44.4	8.7	71.2	564	3.8	L
7	May 11 1968	13 20 05.9	28.5	63.1	602	5.2	L
8	Aug 23 1968	22 36 51.3	22.0	63.5	537	5.8	L,W
9	Aug 23 1968	23 14 52.7	21.8	63.5	541	5.2	L
10	Jul 25 1969	06 06 42.4	25.5	63.3	579	5.5	W
11	Nov 16 1971	22 50 26.0	16.7	64.4	596	4.6	L
12	Jan 12 1972	09 59 10.0	6.9	71.8	586	5.9	N,W
13	Jan 21 1972	19 18 57.0	6.7	71.9	562	5.6	N,W
14	Jan 3 1973	02 58 16.7	27.7	63.3	563	5.6	L
		Region 2 Sea of Okhotsk and East Russia Border					
15	Jun 30 1966	08 59 50.5	43.6N	132.2E	485	5.2	L
16	Sep 10 1966	02 27 48.0	46.6	144.1	335	5.6	L
17	Nov 22 1966	06 29 53.1	48.2	146.7	453	5.6	L
18	Jun 14 1967	03 46 20.3	45.3	136.9	360	4.7	L
19	Oct 9 1967	14 10 57.4	54.0	155.0	393	5.2	L
20	Feb 16 1968	14 23 42.6	49.7	147.7	582	4.7	L
21	Apr 11 1968	06 47 27.4	42.5	131.0	511	5.0	L
22	Jul 21 1968	21 02 31.5	49.7	147.8	576	4.9	L
23	Mar 9 1969	11 35 30.4	48.1	148.3	388	5.1	L
24	Nov 19 1969	08 45 03.3	41.8	133.7	423	5.0	L
25	Dec 18 1969	13 32 05.2	46.3	142.5	344	5.9	L,W
26	Nov 16 1971	01 23 36.0	49.6	147.8	580	4.8	L
27	Mar 6 1972	18 50 18.2	50.2	148.8	592	5.4	L,N,W
28	May 27 1972	04 06 50.4	55.1	156.3	409	5.7	L,N,W
29	Jul 9 1972	13 54 35.3	53.1	154.4	390	5.2	L
30	Aug 2 1972	11 13 22.2	47.4	147.2	351	5.0	L
31	Aug 21 1972	06 23 48.9	49.5	147.0	578	5.9	L,W,N
32	Oct 14 1972	00 00 24.5	48.4	148.7	394	5.6	L,N
33	Dec 27 1972	14 06 09.0	46.3	144.0	342	5.4	L,N
34	Jan 5 1973	13 39 50.4	48.2	146.8	430	5.1	L

Table 1 - continued

Region 3 Honshu and Bonin Islands

Event No.	Date	Origin Time h. m. s.	Lat	Lon	Depth km	Mag	Source
35	Sep 15 1967	08 04 04.4	28.3N	139.6E	438	4.8	L
36	Oct 23 1967	08 27 06.2	28.0	139.6	458	5.4	L
37	Feb 11 1968	12 14 08.6	28.0	139.5	513	4.7	L
38	Feb 28 1968	12 08 01.5	32.9	137.7	349	5.8	L
39	Oct 7 1968	19 20 20.3	26.3	140.6	516	6.1	L
40	Mar 31 1969	19 25 27.2	38.3	134.6	417	5.9	L
41	Jun 1 1969	01 58 03.4	27.5	139.8	482	4.9	L
42	Jun 24 1969	01 21 12.1	31.3	138.3	387	4.5	L
43	Dec 13 1969	03 40 34.8	34.0	137.0	358	5.1	L
44	Aug 11 1971	13 14 15.8	32.1	137.8	386	5.4	N
45	Oct 30 1971	14 16 23.6	32.1	137.7	393	5.6	N
46	Jan 10 1972	19 21 20.5	31.0	137.8	489	5.1	L,N
47	Jul 3 1972	01 19 26.7	18.7	145.1	618	5.7	L
48	Aug 9 1972	15 34 49.6	26.4	140.5	470	5.1	N
49	Nov 13 1972	08 11 48.8	27.9	140.0	372	5.5	N
50	Jan 15 1973	09 02 58.3	27.1	140.1	478	5.8	L
51	Jan 15 1973	09 14 10.7	27.1	140.1	478	5.1	L
52	Jan 31 1973	20 55 53.1	28.2	139.2	498	6.0	L,W

Region 4 New Hebrides Islands

53	Oct 1 1965	13 22 28.4	19.9S	174.5E	546	6.2	L
54	Jan 8 1968	03 17 12.6	13.7	171.5	630	5.2	L
55	Nov 4 1968	09 07 38.5	14.2	172.0	585	5.8	L

Region 5 Tonga and Fiji Islands

56	Dec 9 1965	13 12 55.7	18.0S	178.1W	650	5.6	L
57	Jan 28 1966	09 27 34.4	17.9	178.5	579	5.4	L
58	Apr 8 1967	05 35 17.1	19.9	178.6	616	5.3	L
59	Sep 23 1967	06 56 43.6	21.8	179.7	595	5.4	L
60	Oct 7 1967	10 33 08.2	17.3	178.9	563	4.9	L
61	Oct 9 1967	17 21 49.5	21.1	179.3	654	6.7	L
62	Oct 9 1967	18 33 08.2	21.3	179.3	619	5.1	L
63	Oct 12 1967	06 35 06.7	21.1	179.2	636	5.6	L
64	Nov 10 1967	13 11 18.1	18.0	178.5	592	5.0	L
65	Nov 24 1967	05 42 14.0	16.4	177.9	428	5.4	L
66	Dec 6 1967	05 03 40.8	21.3	178.8	559	5.1	L
67	Jan 20 1968	21 21 31.6	29.9	179.5	349	5.8	L
68	Feb 21 1968	21 05 53.8	20.4	177.9	503	5.5	L
69	Mar 13 1968	20 25 32.1	20.5	178.1	520	5.0	L
70	Apr 9 1968	11 27 39.0	17.8	178.2	650	5.2	L

Table 1 - continued

Event No.	Date	Origin Time h. m. s.	Lat	Lon	Depth km	Mag	Source
71	Jun 18 1968	06 42 21.9	21.7S	179.6W	600	5.0	L
72	Sep 12 1968	22 44 06.5	21.6	179.4	635	5.9	L
73	Sep 16 1968	14 11 29.4	17.4	178.8	583	5.1	L
74	Sep 26 1968	08 41 22.0	17.7	178.5	578	5.1	L
75	Oct 12 1968	19 17 39.9	20.9	178.8	607	5.7	L
76	Oct 29 1968	07 21 16.7	17.8	178.8	567	5.5	L
77	Nov 8 1968	18 27 26.7	19.5	179.2	670	5.2	L
78	Nov 22 1968	15 44 05.0	23.6	180.0	516	5.3	L
79	Dec 12 1968	07 19 44.8	16.0	177.8	431	5.5	L
80	Dec 18 1968	20 03 43.9	19.9	177.6	367	5.5	L
81	Jan 24 1969	02 33 03.5	21.9	179.6	595	5.9	L
82	Jul 19 1969	05 11 43.4	21.7	179.5	659	5.0	L
83	Nov 30 1969	03 33 41.8	17.9	178.6	617	4.5	L
84	Jul 25 1971	16 06 26.0	16.8	178.3	450	5.1	L
85	Sep 19 1971	10 00 19.1	21.3	178.5	545	5.4	L
86	Jan 26 1972	23 00 24.4	20.2	179.0	668	5.7	L
87	Feb 13 1973	15 22 55.1	17.5	178.5	541	5.5	L

Table 2

Results of the Location Scheme of event 40

Phase velocities and equivalent epicenters of P, pdP and P

Phase	P	pdP	pP
Phase velocities (km/sec)	20.85	20.55	19.76
Arrival time	19h 36m 54s	19h 37m 25s	19h 38m 28s
Azimuth	317.0	315.5	315.9
RMS error	0.0667	0.0649	0.0539
Equivalent Epicenters	38.69 N 132.86 E	38.52 N 135.08 E	40.80 N 138.78 E
Geographic Location	Sea of Japan Eastern Asia	Sea of Japan Eastern Asia	Eastern Sea of Japan Japan-Kurlies-Kamchatka
Equivalent epicentral distance (degree)	79.9	78.0	76.4
Equivalent origin time	19h 24m 47s	19h 25m 22s	19h 26m 40s

Table 3

Amplitude ratio and time interval between pdP and pP in South America region

Amplitude ratio and time interval between precursors and pP are listed. The letters following the time interval in column 5, 7 and 9 represent the qualities of the precursors (G: good, F: fair, P: poor).

Event No.	Source	Process	Distance (deg)	$pP\text{-}pd_1P$ (sec)	$\frac{A_{pd_1P}}{A_{pP}}$	$pP\text{-}pd_2P$ (sec)	$\frac{A_{pd_2P}}{A_{pP}}$	$pP\text{-}pd_3P$ (sec)	$\frac{A_{pd_3P}}{A_{pP}}$	$\frac{A_{pP}}{A_P}$
1.	LASA		83.0	30(F)	0.3	65(G)	0.1	-	-	0.5
2.	LASA	Beam	83.4	29(F)	0.15	-	0.3	72(F)	0.22	0.3
	LUB		70.8	27(F)	0.4	56(G)	-	70(F)	0.3	0.13
								80(G)	0.2	
	OXF		66.3	32(F)	0.2	54(F)	0.7	70(G)	-	0.42
	AAM		71.8	32(F)	0.3	67(P)	0.3	-	-	1
	PRE		79.8	28(F)	0.15	66(F)	0.2	-	-	0.4
						56(P)	0.75	-	-	
	JCT		67.3	28(F)	0.3	67(F)	0.55	78(F)	0.2	0.2
	DUG		81.5	31(G)	0.2	66(F)	0.15	-	-	0.86
	TOL		86.6	32(G)	0.5	55(G)	0.45	72(G)	0.3	0.45
	PTO		84.8	27(G)	0.15	58(F)	0.2	70(F)	0.15	0.25
	BLA		66.2	-	-	57(G)	0.1	72(G)	0.2	0.45
	GSC		80.2	-	-	60(F)	0.15	80(F)	0.2	1.1
3.	SCP		49.9	-	-	55(F)	0.1	-	-	0.25
	PRE		94.7	25(P)	0.35	57(F)	0.1	72(F)	0.2	0.3
								83(G)	0.35	0.3
	TRI		93.0	-	0.35	60(F)	0.2	72(F)	0.6	0.3
								83(G)	1.00	0.3
	STU		90.6	33(G)	0.45	60(F)	0.35	75(F)	0.5	0.36
	LOR		86.7	26(F)	0.25	68(F)	0.25	82(F)	0.3	0.45
	BKS		66.5	32(G)	0.80	65(F)	0.85	81(G)	1.25	0.15
	GSC		61.4	30(G)	0.53	65(F)	0.65	80(G)	0.8	0.29

Table 3 (continued)

Event No.	Source	Process	Distance	$pP\text{-}pd_1P$ (sec)	$\frac{A_{pd_1P}}{A_{pP}}$	$pP\text{-}pd_2P$ (sec)	$\frac{A_{pd_2P}}{A_{pP}}$	$pP\text{-}pd_3P$ (sec)	$\frac{A_{pd_3P}}{A_{pP}}$	$\frac{A_{pP}}{A_P}$
3. (cont)	WES		51.1	-	-	55(G) 65(G)	1.2 0.86	80(G)	0.7	0.3
	CMC		82.7	-	-	65(F)	0.2	81(G)	0.3	0.8
4.	LASA	Beam Location VESPA	83.7	27.5	0.35	66.5(F)	0.2	-	-	0.73
5.	LASA	Beam	83.7	34(F)	0.2	67.2(F)	0.19	-	-	0.6
6.	LASA	VESPA	63.4	32(G)	1.5	67(G)	1.0	-	-	0.09
7.	LASA		84.6	26(P)	0.5	-	-	70(P)	0.25	0.09
8.	LASA	Beam Location	78.5	32(G)	0.3	56(G) 69(F)	0.4 0.5	-	-	0.65
	BLA		61.1	30(F)	0.2	51(F)	0.4	70(F) 80(F)	0.3 0.51	0.6
	BKS		81.2	-	-	55(G)	0.4	-	-	0.75
	MAL		80.7	-	-	60(G)	0.3	74(P)	0.15	1.1
	BUL		84.5	35(G)	0.42	56(G)	0.36	70(F)	0.2	0.36
	GDH		91.3	-	-	55(P)	0.2	81(F)	0.3	1.5
9.	LASA	Beam VESPA	78.3	31(G)	0.09	58(G)	0.37	-	-	0.08
10.	OGD		67.1	-	-	63(F)	1.5	71(G)	1.5	0.13
	SBA		72.8	32(G)	0.2	54(P) 63(G)	0.05 0.3	86(F)	0.15	1.0
11.	LASA	Beam VESPA	73.5	28(G)	0.2	-	-	70(G)	0.35	0.4

Table 3 ---- (Continued)

Event	Source	Process	Distance	$pP\text{-}pd_1P$	$\frac{A_{pd_1P}}{A_{pP}}$	$pP\text{-}pd_2P$	$\frac{A_{pd_2P}}{A_{pP}}$	$pP\text{-}pd_3P$	$\frac{A_{pd_3P}}{A_{pP}}$	$\frac{A_{pP}}{A_P}$
12.	NORSAR	Beam VESPA	92.2	-	-	66(P)	0.34	-	-	0.11
13.	NORSAR	Beam	92.2	-	-	64(P)	0.45	-	-	0.15
	OGD		49.6	-	-	51(P)	1.2	70(F)	1.3	0.3
14.	LASA	Beam	83.8	27(P)	0.6	65(P)	0.8	-	-	0.16

Table 4

Amplitude ratio and time interval between pdP and pP in Sea of Okhotsk region

Amplitude ratio and time interval between precursors and pP are listed The letters following the time interval in column 5, 7 and 9 represent the qualities of the precursors (G : good, F : fair, P : poor)

Event No.	Source	Process	Distance (deg)	$pP\text{-}pd_1P$ (sec)	$\frac{A_{pd_1P}}{A_{pP}}$	$pP\text{-}pd_2P$ (sec)	$\frac{A_{pd_2P}}{A_{pP}}$	$pP\text{-}pd_3P$ (sec)	$\frac{A_{pd_3P}}{A_{pP}}$	$\frac{A_{pP}}{A_P}$
15.	LASA	Beam VESPA Location	76.3	21(F)	0.25	60(G)	0.25	79(G)	0.4	0.7

Table 4 ---- (Continued)

Event No.	Source	Process	Distance (deg)	$pP\text{-}pd_1P$ (sec)	$\frac{A_{pd_1P}}{A_{pP}}$	$pP\text{-}pd_2P$ (sec)	$\frac{A_{pd_2P}}{A_{pP}}$	$pP\text{-}pd_3P$ (sec)	$\frac{A_{pd_3P}}{A_{pP}}$	$\frac{A_{pP}}{A_P}$
16.	LASA		68.6	20(F)	0.4	52(P)	0.35	-	-	0.09
17.	LASA	Beam	66.2	20(P)	0.2	63(F)	0.3	-	-	0.23
18.	LASA	Beam VESPA	72.9	-	-	51(G)	0.3	-	-	0.15
19.	LASA	Beam Location	58.3	-	-	56(G)	0.25	72(G)	0.25	0.3
20.	LASA	Beam Location	64.7	-	-	64(F)	0.25	80(F)	0.25	1.0
21.	LASA	Beam	77.7	32(F)	0.2	67(G)	0.25	84(G)	0.5	0.2
22.	LASA	Beam Location	64.6	34(P)	0.1	56(G)	0.2	83(G)	0.2	0.4
23.	LASA	Beam	65.5	-	-	48(F)	0.5	72(P)	0.6	0.12
24.	LASA	Beam Location	77.1	34(G)	0.3	53(F) 62(G)	0.5 0.4	82(G)	0.5	0.3
25.	LASA	Beam VESPA	69.5	19(P)	1.0	48(F) 52(F)	1.0 0.8	-	-	0.2
	DUG		70.1	30(F)	0.7	60(F)	0.9	70(F)	0.6	0.17
	KEV		55.2	-	-	60(F)	0.9	-	-	0.2
26.	LASA	Beam	64.6	21(F)	0.15	54(F)	0.2	-	-	0.5
27.	LASA	Beam	63.8	-	-	60(F)	0.3	-	-	0.15

Table 4 ---- (Continued)

Event No.	Source	Process	Distance (deg)	$pP\text{-}pd_1P$ (sec)	$\frac{A_{pd_1P}}{A_{pP}}$	$pP\text{-}pd_2P$ (sec)	$\frac{A_{pd_2P}}{A_{pP}}$	$pP\text{-}pd_3P$ (sec)	$\frac{A_{pd_3P}}{A_{pP}}$	$\frac{A_{pP}}{A_P}$
27.	NORSAR	Beam	64.5	25(P)	0.7	58(P)	1.0	74(P)	0.8	0.1
	BKS		61.5	21(G)	0.4	55(G)	1.2	79(G)	1.4	0.4
	DUG		61.1	-	-	49(G)	0.16	82(G)	1.5	o.35
	IST		75.2	-	-	60(P)	1.0	-	-	0.4
	KEV		53.2	-	-	45(F)	1.2	-	-	0.2
						60(F)	1.2			
	NUR		60.9	-	-	60(G)	0.3	-	-	0.35
	QUE		62.5	32(F)	0.6	55(F)	0.8	-	-	0.25
						64(F)	1.0			
	UME		59.5	-	-	50(P)	0.5	-	-	0.1
28.	LASA	Beam VESPA Location	57.29	32(G)	0.5	62(G)	1.1	-	-	0.25
	NORSAR	Beam VESPA	61.33	31(F)	1.1	60(G)	1.1	-	-	0.15
	NUR		58.6	26(F)	0.45	58(F)	0.8	-	-	0.25
	GSC		60.3	-	-	60(F)	0.75	-	-	0.3
	ATU		78.9	25(F)	0.25	61(G)	0.7	-	-	0.35
	WEL		74.9	25(F)	0.2	62(F)	0.15	-	-	1.1
	KEV		50.3	-	-	45(F)	1.0	-	-	0.25
	JER		79.9	-	-	63(F)	1.1	-	-	0.15
	IST		74.3	-	-	62(F)	1.0	-	-	0.25
	ALQ		66.0	-	-	56(F)	0.6	-	-	0.3
29.	LASA	Beam	53.24	29(F)	0.3	48(F)	0.5	72(G)	0.5	0.1
30.	LASA	Beam VESPA	66.46	30(F)	0.8	56(P)	0.8	-	-	0.1
31.	LASA	Beam VESPA	65.1	32(G)	0.2	60(G)	0.3	74(G)	0.5	0.4

Table 4 ----- (Continued)

Event No.	Source	Process	Distance (deg)	$pP\text{-}pd_1P$ (sec)	$\frac{A_{pd_1P}}{A_{pP}}$	$pP\text{-}pd_2P$ (sec)	$\frac{A_{pd_2P}}{A_{pP}}$	$pP\text{-}pd_3P$ (sec)	$\frac{A_{pd_3P}}{A_{pP}}$	$\frac{A_{pP}}{A_P}$
31.	NORSAR	Beam VESPA	64.0	30(G)	0.28	51(G) 68(G)	0.5 0.8	81(G)	0.8	0.3
	ALQ		72.4	-	-	53(G)	0.32	75(G)	0.31	0.46
	TER		79.5	-	-	62(F)	0.35	-	-	0.25
	NUR		60.2	23(F)	0.7	49(F)	0.6	-	-	0.14
	OGD		80.7	-	-	60(F)	0.5	82(G)	0. 8	0.25
	SHI		70.2	-	-	55(G)	0.5	78(F)	0.7	0.45
	STU		75.7	-	-	62(F)	0.5	-	-	0.21
	TRI		77.7	-	-	60(G)	0.7	83(G)	0.8	0.19
32.	LASA	Beam Location	65.07	32(G)	0.09	60(G)	0.2	-	-	0.4
	NORSAR	Beam	64.27	32(P)	1.0	51(P)	1.0	-	-	0.1
33.	LASA	Beam VESPA	68.8	34(F)	0.12	64(F)	0.25	-	-	0.8
	NORSAR		64.0	23(F)	0.5	55(F)	0.4	-	-	0.8
34	LASA	Beam VESPA	66.15	-	-	58(P)	1.0	75(P)	0.45	0.02

Table 5

Amplitude ratio and time interval between pdP and pP in Bonin Islands region

Amplitude ratio and time interval between precusors and pP are listed. The letters following the time interval in colume 5,7 and 9 represent the qualities of the precusors (G: good, F: fair, P: poor).

Event No.	Source	Process	Distance (deg)	$pP\text{-}pd_1P$ (sec)	$\frac{A_{pd_1P}}{A_{pP}}$	$pP\text{-}pd_2P$ (sec)	$\frac{A_{pd_2P}}{A_{pP}}$	$pP\text{-}pd_3P$ (sec)	$\frac{A_{pd_3P}}{A_{pP}}$	$\frac{A_{pP}}{A_P}$
35.	LASA	Beam VESPA	84.6	20(P)	0.25	60(P)	0.25	-	-	0.15
36.	LASA	Beam	85.0	22(F)	0.3	60(F)	0.28	80(F)	0.32	0.35
37.	LASA	Beam Location	84.0	-	-	45(F) 60(F)	0.14 0.15	91(G)	0.18	0.9
38.	LASA	Beam VESPA	82.1	20(F)	0.3	48(F) 56(F)	0.55 0.45	-	-	0.2
39.	LASA	Beam Location	85.5	30(F)	0.35	60(F)	0.3	80(G)	0.4	1.0
40.	LASA	Beam VESPA	79.4	29(F)	0.3	41(F) 57(F)	0.4 0.2	72(F)	0.4	0.5
41.	LASA		85.1	-	-	54(P) 62(P)	0.4 0.5	-	-	0.8
42.	LASA		81.3	29(P)	0.4	-	-	-	-	0.1
43.	LASA	Beam	81.6	-	-	40(F) 58(F)	0.9 0.7	-	-	0.08

Table 5 ---- Continue

Event No.	Source	Process	Distance (deg)	$pP\text{-}pd_1P$ (sec)	$\frac{A_{pd_1P}}{A_{pP}}$	$pP\text{-}pd_2P$ (sec)	$\frac{A_{pd_2P}}{A_{pP}}$	$pP\text{-}pd_3P$ (sec)	$\frac{A_{pd_3P}}{A_{pP}}$	$\frac{A_{pP}}{A_P}$
44.	NORSAR	Beam Location	77.8	29(G)	0.6	54(G)	1.0	70(G)	1.0	0.15
45.	NORSAR	Beam	77.8	30(F)	0.9	57(G)	1.0	73(F)	0.8	0.1
46	NORSAR	Beam VESPA	78.6	-	-	64(G)	0.6	74(F) 84(F)	0.6 0.8	0.1
47.	LASA	Beam	88.74	31(F)	0.6	55(P) 66(P)	0.3 0.4	84(G)	1.0	0.3
48.	NORSAR	Beam Location	83.99	-	-	-	-	70(F) 90(G)	1.0	0.1
49.	NORSAR	Beam VESPA	82.47	-	-	46(F) 60(G)	1.4 1.2	-	-	0.9
50.	LASA	Beam VESPA	85.3	30(F)	0.4	56(F)	0.3	75(G)	0.7	0.2
	NORSAR	Beam	83.21	32(F)	1.1	56(F)	1.3	74(G)	2.0	0.15
51.	LASA	Beam	83.3	28(P)	0.1	54(F)	0.3	71(G)	0.5	0.14
52.	LASA	Beam VESPA	84.9	29(F)	0.2	60(F)	0.17	72(F)	0.4	0.4
	NORSAR	Beam Location	81.9	28(G)	0.4	60(G)	0.3	70(G)	0.4	0.4
	IST		84.1	-	-	60(F)	0.5	-	-	1.0
	NOR		78.8	-	-	65(F)	0.4	-	-	0.85
	NUR		75.5	-	-	60(F)	0.25	-	-	0.65
	TAR		74.8	30(P)	1.0	-	-	70(P)	1.0	1.0
	UME		75.0	-	-	64(G)	0.75	-	-	0.75

Table 6

Amplitude ratio and time interval
between pdP and pP in New Hebrides region

Amplitude ratio and time interval between precursors and pP are listed
The letters following the time interval in column 5, 7 and 9 represent
the qualities of the precursors (G : good, F : fair, P : poor)

Event No.	Source	Process	Distance (deg)	pP -pd_1P (sec)	$\frac{A_{pd_1P}}{A_{pP}}$	pP-pd_2P (sec)	$\frac{A_{pd_2P}}{A_{pP}}$	pP-pd_3P (sec)	$\frac{A_{pd_3P}}{A_{pP}}$	$\frac{A_{pP}}{A_P}$
53.	LASA	Beam VESPA Location	97.1	18(P)	0.07	60(G)	0.2	91(G)	0.3	0.4
54.	LASA	Beam Location	94.7	-	-	62(G)	0.15	82(G)	0.3	0.4
55.	LASA	Beam VESPA Location	94.7	-	-	56(G)	0.13	70(G)	0.32	0.5

Table 7

Amplitude ratio and time interval between pdP and pP in Fiji- Tonga region

Amplitude ratio and time interval between precusors and pP are listed The letters following the time interval in column 5,7 and 9 represent the qualities of the precusors (G : good, F : fair, P : poor).

Event No.	Source	Process	Distance (deg)	$pP\text{-}pd_1P$ (sec)	$\frac{A_{pd_1P}}{A_{pP}}$	$pP\text{-}pd_2P$ (sec)	$\frac{A_{pd_2P}}{A_{pP}}$	$pP\text{-}pd_3P$ (sec)	$\frac{A_{pd_3P}}{A_{pP}}$	$\frac{A_{pP}}{A_P}$
56.	LASA	Beam VESPA	91.1	-	-	57(F)	0.9	78(F) 95(F)	0.8 0.7	0.1
57.	LASA	Beam	91.3	-	-	-	-	71(P)	0.6	0.05
58.	LASA	Beam VESPA	92.9	-	-	54(F) 67(F)	0.45 0.25	91(F)	0.3	0.3
59.	LASA	Beam	94.9	-	-	58.5(F)	0.25	80(F)	0.15	0.4
60.	LASA	Beam	91.1	35(F)	0.25	51(F) 65(F)	0.3 0.25	-	-	0.3
61.	LASA	Beam	94.2	-	-	55(P)	0.15	70(G) 85(F)	0.25 0.34	0.8
62.	LASA	Beam	94.3	-	-	62(P)	0.2	82(P)	0.125	1.0
63.	LASA	Beam VESPA Location	94.1	-	-	40(F) 64(G)	0.08 0.06	85(G)	0.08	1.0
64.	LASA	Beam	91.3	-	-	-	-	80(P)	1.0	0.05
65.	LASA	Beam Location	89.8	29(G)	0.5	45(G) 62(G)	0.5 0.5			0.15

Table 7 ---- Continue

Event No.	Source	Process	Distance (deg)	$pP\text{-}pd_1P$ (sec)	$\frac{A_{pd_1P}}{A_{pP}}$	$pP\text{-}pd_2P$ (sec)	$\frac{A_{pd_2P}}{A_{pP}}$	$pP\text{-}pd_3P$ (sec)	$\frac{A_{pd_3P}}{A_{pP}}$	$\frac{A_{pP}}{A_P}$
66.	LASA	Beam	94.0	-	-	45(P)	0.1	74(F) 83(F)	0.15 0.2	0.4
67.	LASA		100.8	25(F)	1.5	52(P) 65(P)	1.3 1.1			0.3
68.	LASA		92.8	-	-	45(P) 60(P)	1.1 1.23	70(P)	1.31	0.15
69.	LASA	Beam VESPA	93.0	25(P)	0.2	54(F)	0.14	87(F)	0.2	1.5
70.	LASA	Beam	91.0	-	-	55(F)	0.3	70(P) 90(G)	0.15 0.4	0.14
71.	LASA	Beam	94.8	-	-	-	-	74(P) 87(P)	0.1 0.15	1.2
72.	LASA	Beam Location	94.6	35(F)	0.2	54(G) 66(F)	0.35 0.2	78(G)	0.25	0.14
73.	LASA	Beam	91.1	-	-	65(P)	0.1	-	-	0.9
74.	LASA	Beam Location	93.7	29(F)	0.1	53(G)	0.4	73(F) 90(G)	0.25 0.35	0.85
75.	LASA	Beam VESPA	93.7	-	-	40(F) 57(P)	0.2 0.25	82(P)	0.15	0.3
76.	LASA	Beam	91.4	25(P)	0.15	40(F) 51(F)	0.25 0.25	87(P)	0.15	0.07

Table 7 ---- Continue

Event No.	Source	Process	Distance (deg)	pP-pd$_1$P (sec)	$\frac{A_{pd_1P}}{A_{pP}}$	pP-pd$_2$P (sec)	$\frac{A_{pd_2P}}{A_{pP}}$	pP-pd$_3$P (sec)	$\frac{A_{pd_3P}}{A_{pP}}$	$\frac{A_{pP}}{A_P}$
77.	LASA	Beam Location	92.9	-	-	55(F)	0.25	80(G)	0.12	0.15
78.	LASA	Beam	96.4	29(P)	0.5	52(P)	0.4	70(P)	0.5	0.23
79.	LASA	Beam Location	89.4	30(F)	0.2	50(F)	0.15	70(G) 82(G)	0.3	0.25
80.	LASA	Beam VESPA	92.2	30(F) 39(F)	0.3 0.35	56(F) 62 (F)	0.45	72(F)	0.3	0.25
81.	LASA	Beam Location	94.9	-	-	54(F)	0.1	72(G)	0.1	2.0
82.	LASA	Beam Location	94.6	33(G)	0.4	55(F)	0.5	72(G)	0.5	0.16
83.	LASA		91.3	31(P)	0.8	52(F)	1.2	-	-	0.1
84.	LASA	Beam VESPA	90.0	-	-	55(G)	0.2	71(G) 80(G)	0.3 0.45	0.3
85.	LASA	Beam	93.8	31(P)	0.2	52(P) 60(F)	0.1 0.3	-	-	0.6
86.	LASA	Beam Location	93.0	-	-	60(G)	0.3	70(G)	0.4	0.3
87.	LASA	Beam	93.97	28(P)	0.07	59(F)	0.09	70(G)	0.1	0.2

Table 8

Characteristics of the estimated reflectors

Region	Range of discontinuity (km)	Subregion	Reflector (km)	Impedance ratio	Velocity gradient (%)	Density gradient (%)
South America	100-140	Salta, Argentina West Brazil	120	1.26-1.19	12.5-9.4	9.1-7.3
		Santiago Del Estero, Argentina	120	1.30	13.8	10.5
	240-260	Salta, Argentina	245	1.29	13.8	10.5
	280-320	Santiago,Del Estero, Argentina	280	1.18	8.8	6.9
Sea of Okhotsk	80-140	Russia Border	80	1.203	10.0	8.0
		Sea of Okhotsk	140	1.1	5.3	4.1
	220-290	Russia border	265	1.17	8.0	6.9
		Sea of Okhotsk	250	1.19	9.3	7.5
	320-400	Russia border	354	1.22	10.5	8.6
		Sea of Okhotsk	390	1.16	8 2	6.3

Table 8 --- Continue

Region	Range of Discontinuity (km)	Subregion	Reflector (km)	Impedance ratio	Velocity gradient (%)	Density gradient (%)
Bonin Islands	100-140	Sea of Japan	120	1.24	11.5	8.9
		Bonin Islands	125	1.27	12.8	9.6
	160-200	Sea of Japan	170	1.22	10.6	8.2
		Bonin Islands	170	1.12	6.1	4.2
	230-260	Sea of Japan	245	1.20	9.7	7.6
		Bonin Islands	250	1.17	8.7	6.8
	300-330	Sea of Japan	315	1.15	7.2	5.3
	350-400	Sea of Japan	350	1.19	9.2	7.4
Fiji-Tonga and New Hebrides	110-140	Fiji Islands	130	1.23	11.0	9.0
	160-180	Fiji Islands	170	1.10	5.2	4.01
	230-260	Tonga	260	1.16	8.0	6.3
		New Hebrides	250	1.20	9.5	7.8
	280-310	Fiji Islands	285	1.18	8.9	7.1
	320-400	Tonga	400	1.19	9.3	7.1
		New Hebrides	400	1.20	9.7	7.9

Figure 1. Short period vertical records of pP and precursors of event 8 at LASA. Twelve traces are the Subarray Sums of three outer rings.

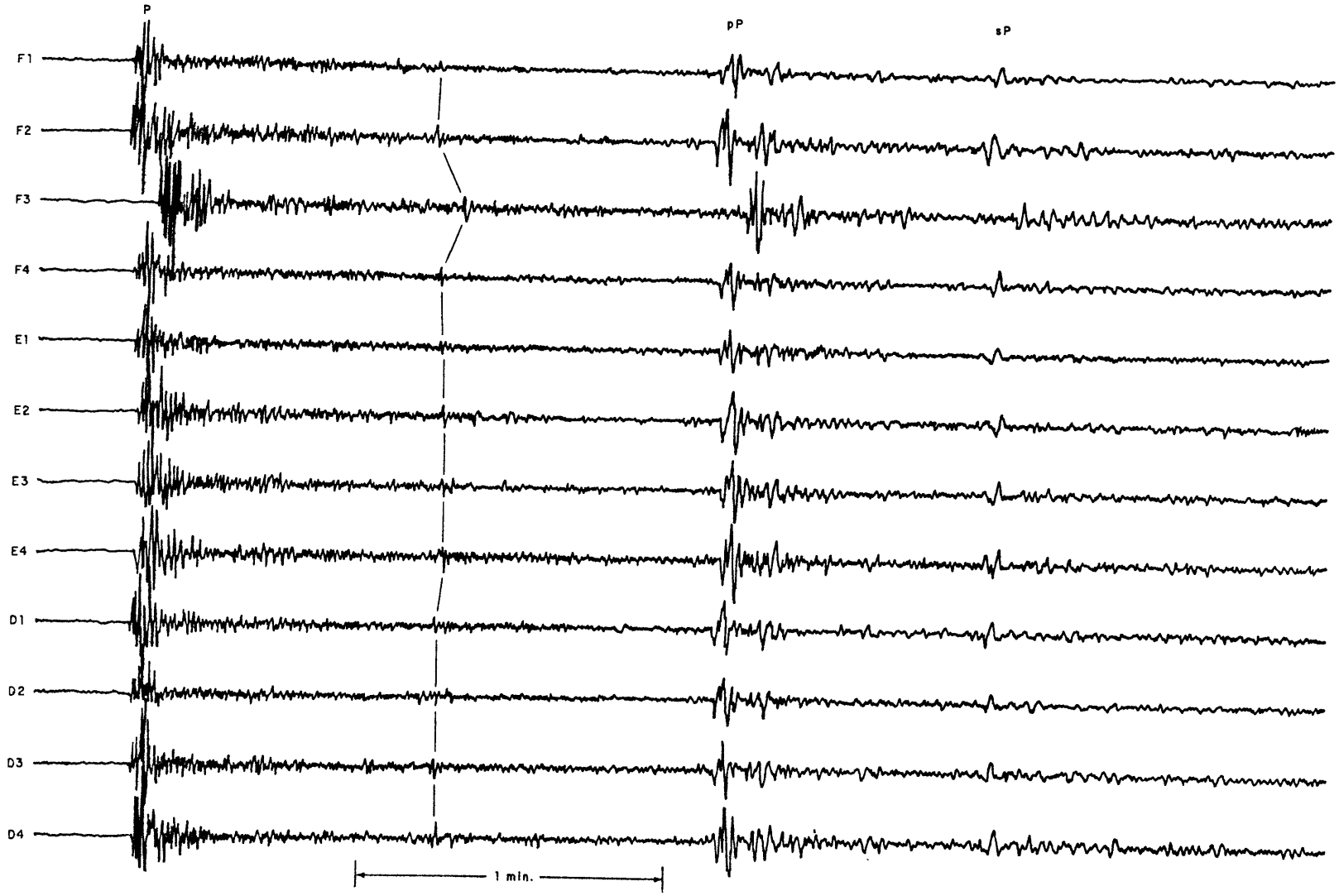
P
pP
sP
F1
F2
F3
F4
E1
E2
E3
E4
D1
D2
D3
D4
1 min.

Figure 2. Seismometer locations at LASA as first installed. Short period seismometers were located at each site-a total of 525. Twenty-one three-component long period seismometers were placed at the center of the subarrays.

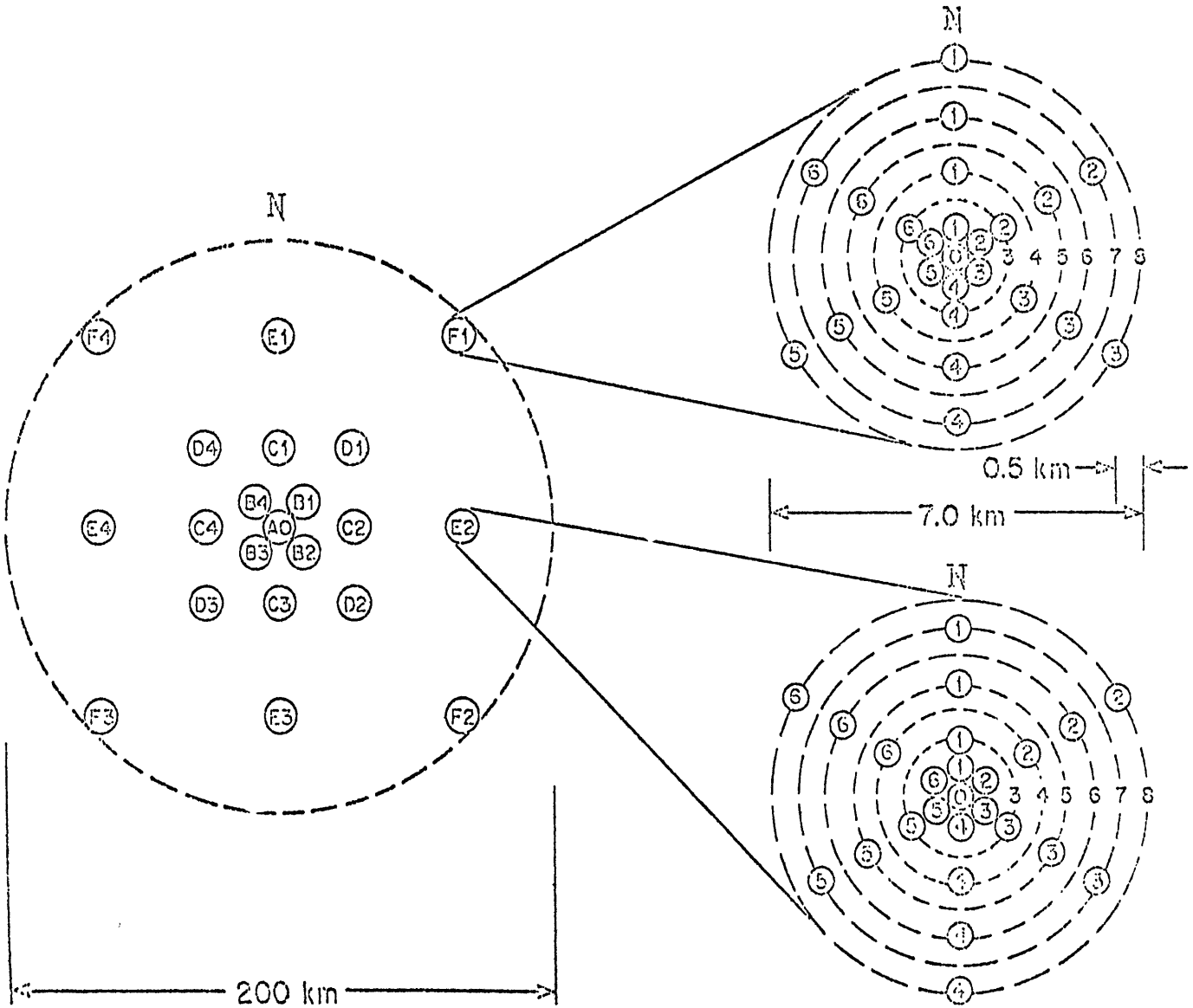
N
F4
E1
F1
D4
C1
D1
B4
B1
E4
C4
A0
C2
E2
B3
B2
D3
C3
D2
F3
E3
F2
200 km
N
0 1 2 3 4 5 6 7 8
0.5 km
7.0 km
N
0 1 2 3 4 5 6 7 8

Figure 3. Short period seismometer locations at NORSAR. In each subarray, there is also one three-component long period seismometer.

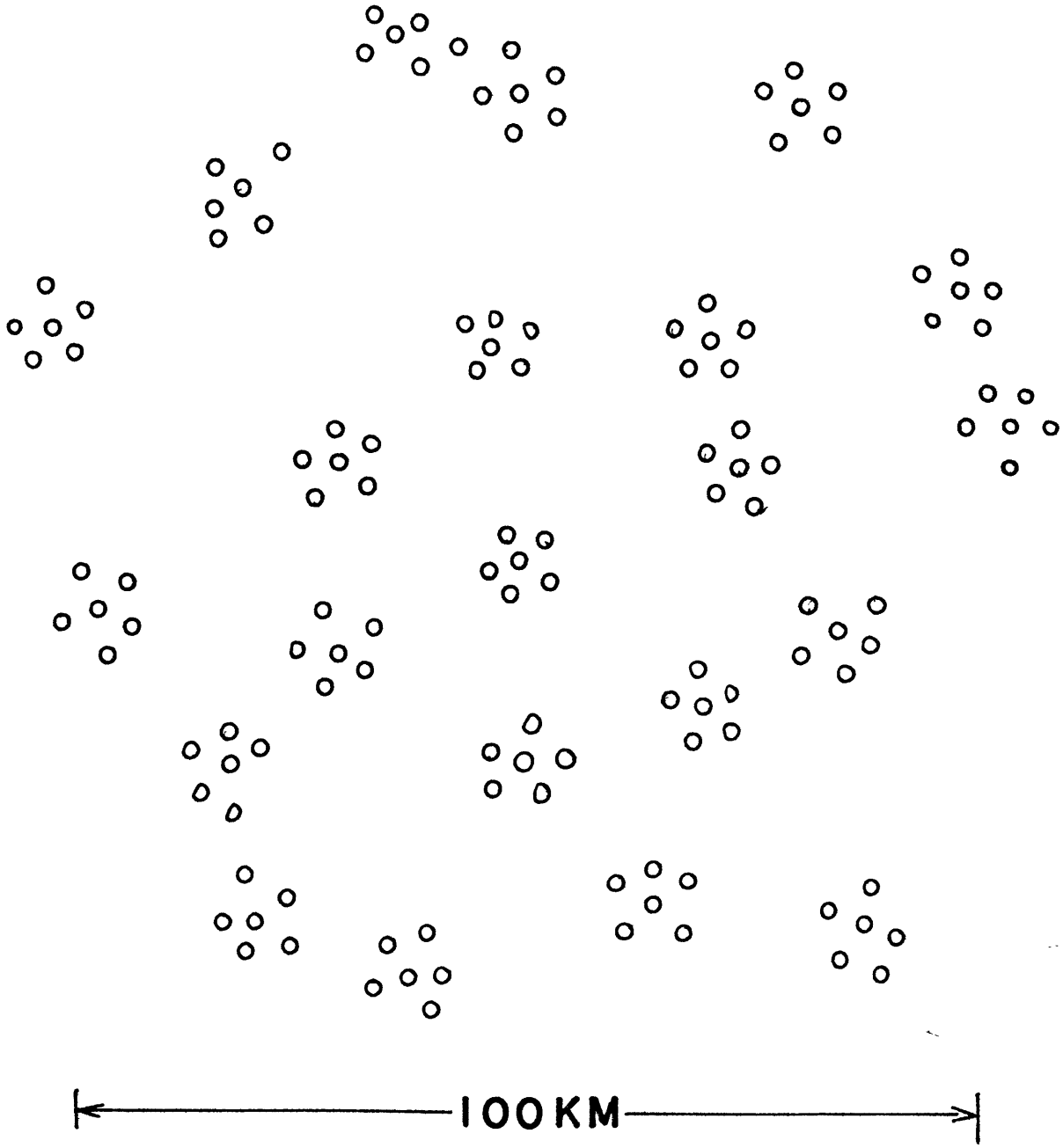
100 KM

Figure 4. Short period vertical records of pP and precursors of event 24 at LASA. The first line is the beam trace of 21 Subarray Sums. Other traces are the Subarray Sums of two outer rings.

Figure 5. Beam traces of 21 Subarray Sums at LASA.
Events are No. 37, 84, 8, and 4 in order.

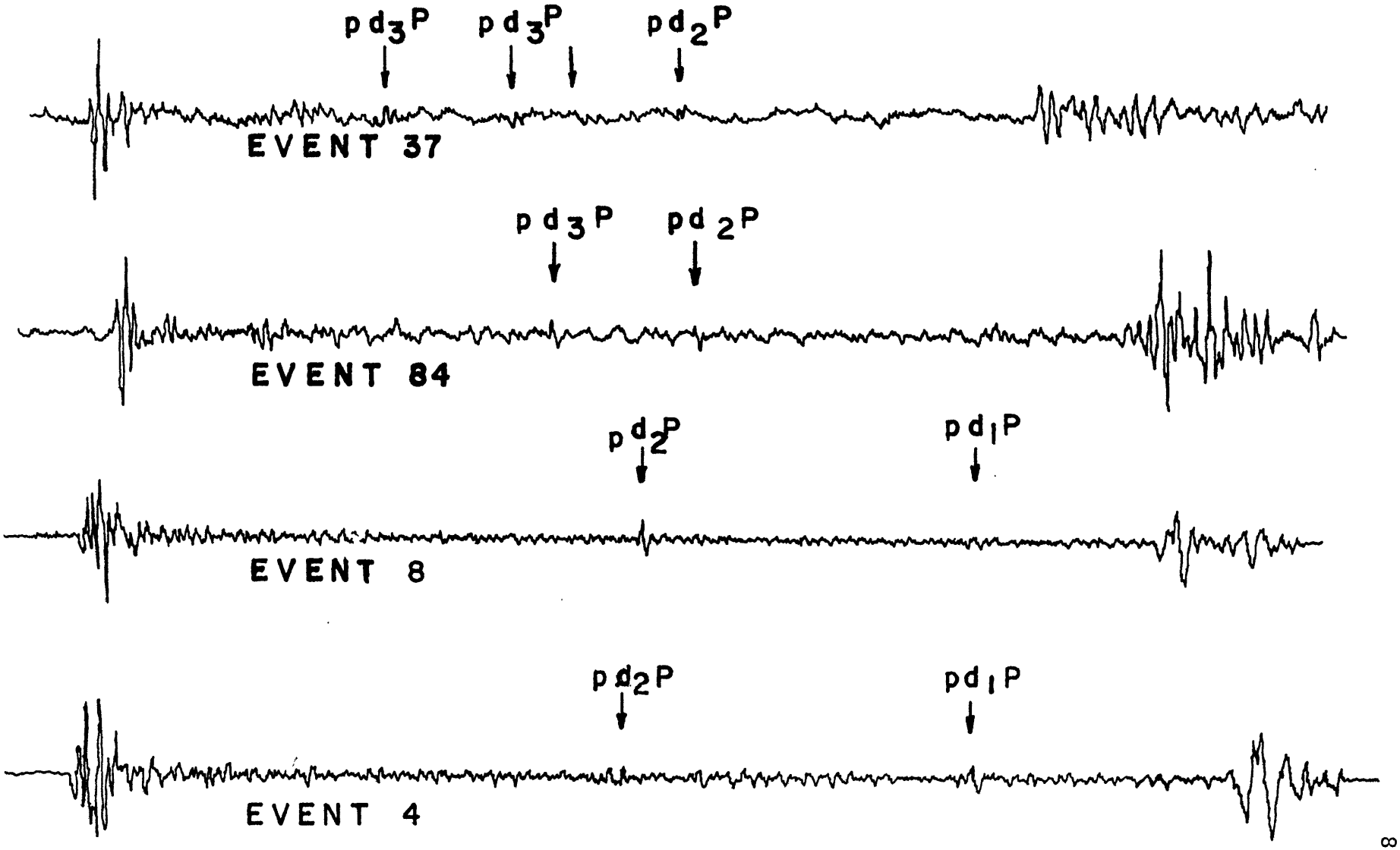
pd3P
pd3P
pd2P
EVENT 37
pd3P
pd2P
EVENT 84
pd2P
pd1P
EVENT 8
pd2P
pd1P
EVENT 4

Figure 6. Vespagram and six Subarray Sums of event 75.

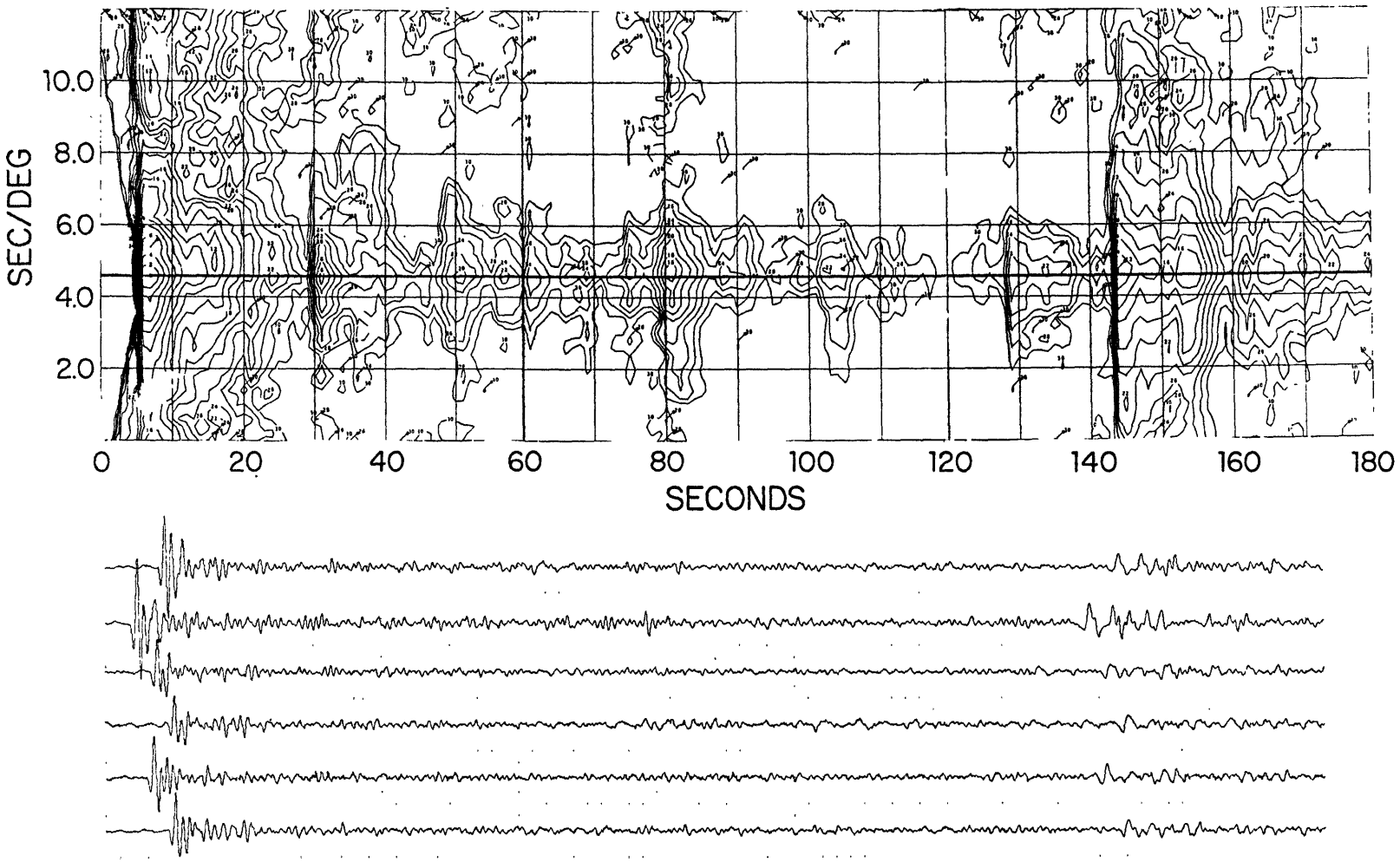

12 OCT 1967 21°1 S m_b = 5.6
06H 35M 6.7S 175°2W H = 636

Figure 7. Ray paths and equivalent epicenters of P, pdP and pP phases

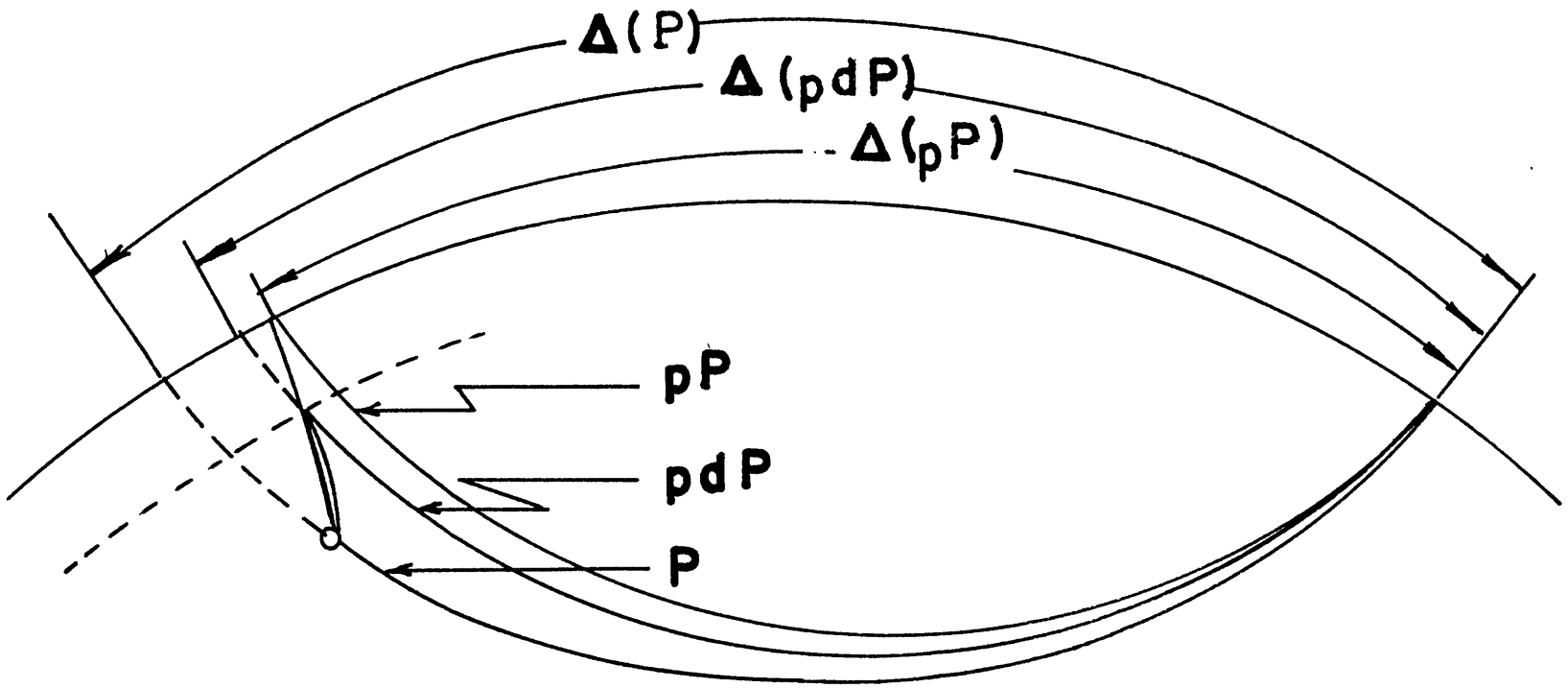

$$\Delta(P) > \Delta(pdP) > \Delta(pP)$$

Figure 8. Travel time interval between precursors and pP in South America region. The coordinate is the epicentral distance. Solid circle : good, Open circle : fair, Cross : poor.

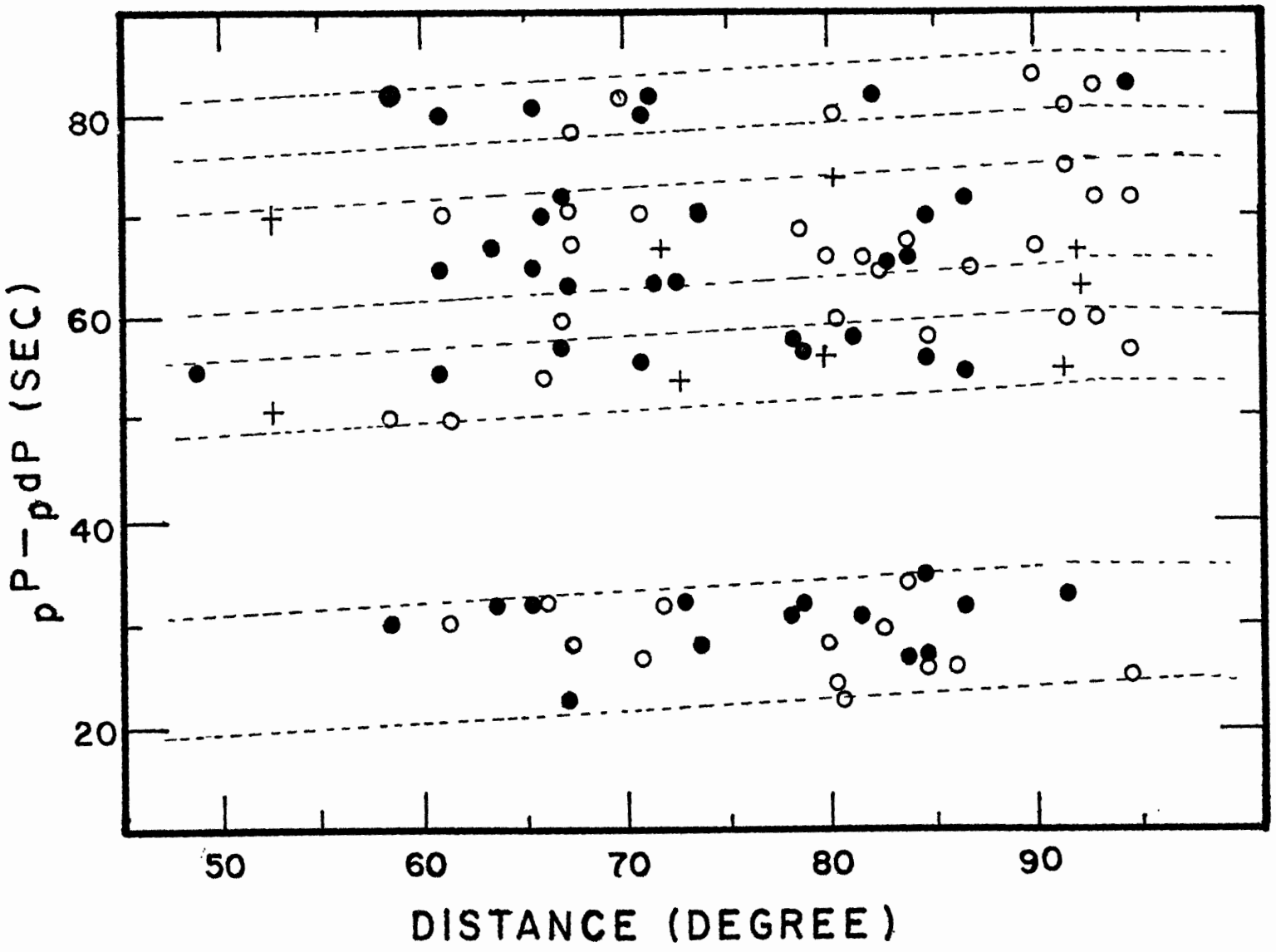
80
60
40
20
$p^P - p^{dP}$ (SEC)
50
60
70
80
90
DISTANCE (DEGREE)

Figure 9. Travel time interval between precursors and pP in the Sea of Okhotsk region. The coordinate is the epicentral distance.
Solid circle : good, open circle : fair, cross : poor.

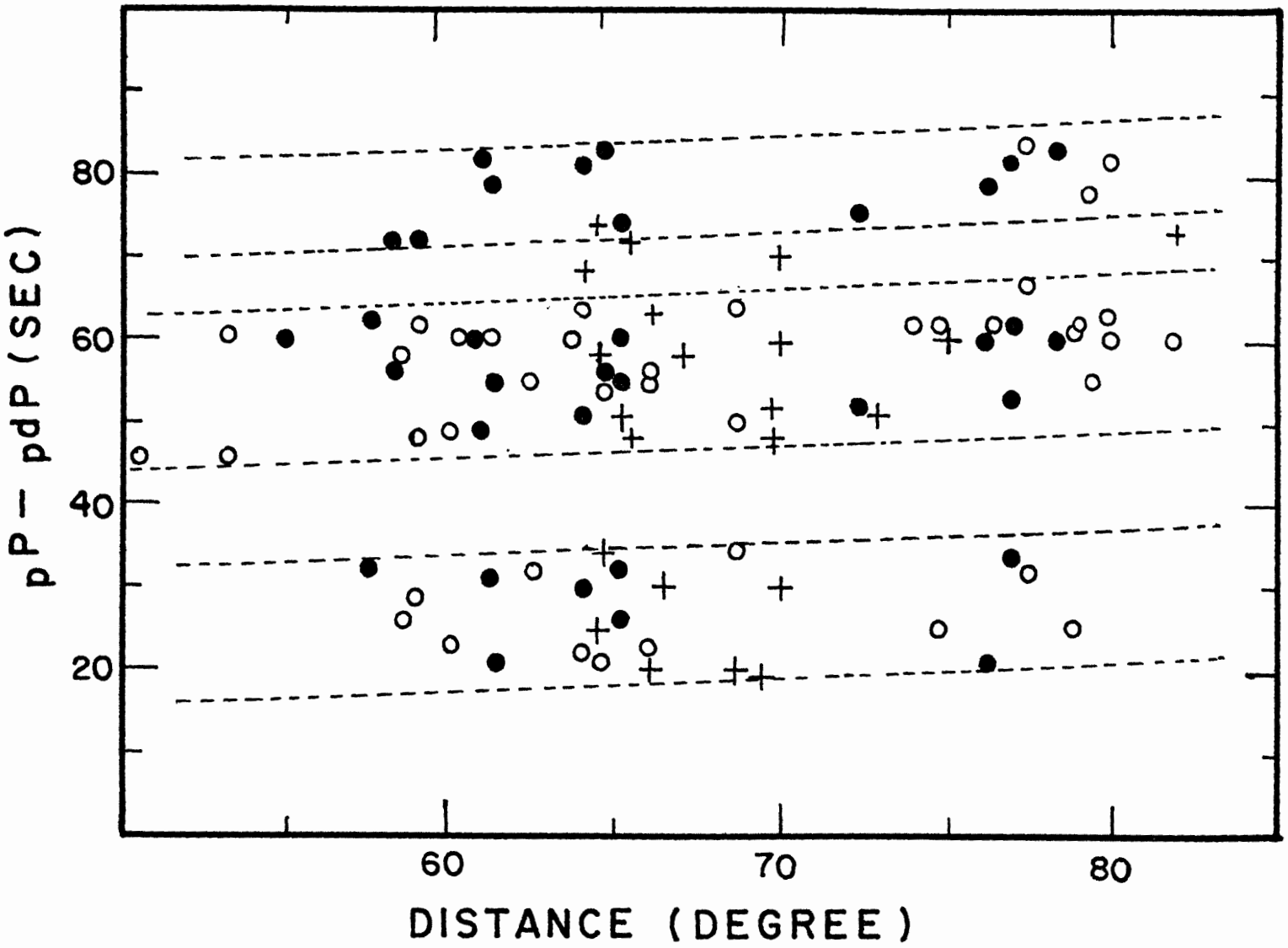
pP − pdP (SEC)
80
60
40
20
60
70
80
DISTANCE (DEGREE)

Figure 10. Travel time interval between precursors and pP in Bonin Islands region. The coordinate is the epicentral distance.
Solid circle : good, open circle : fair, cross : poor.

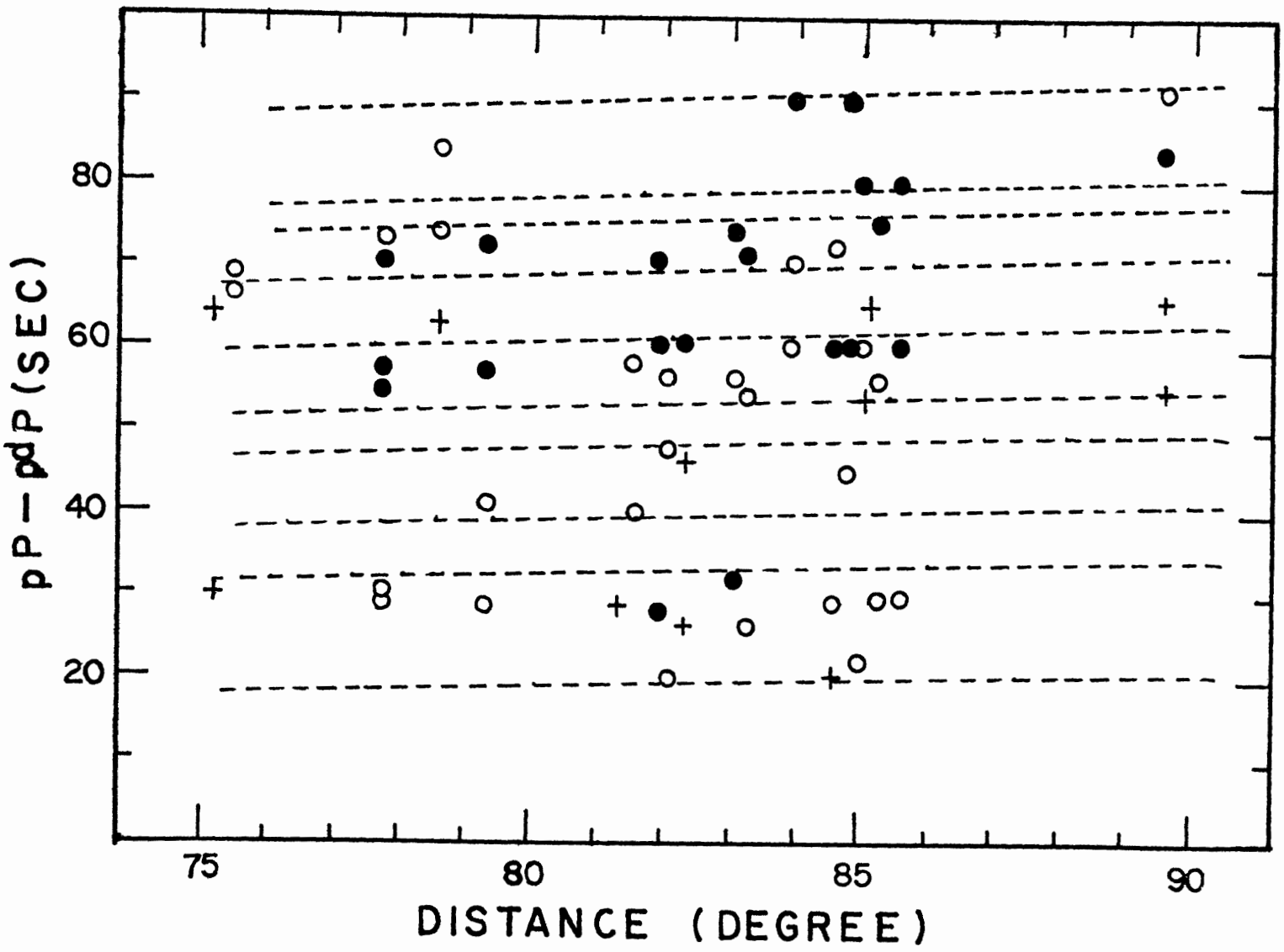
pP − pdP (SEC)
80
60
40
20
75
80
85
90
DISTANCE (DEGREE)

Figure 11. Travel time interval between precursors and pP in New Hebrides and Fiji-Tonga regions. The coordinate is the epicentral distance. Solid circle : good, open circle : fair, cross : poor.

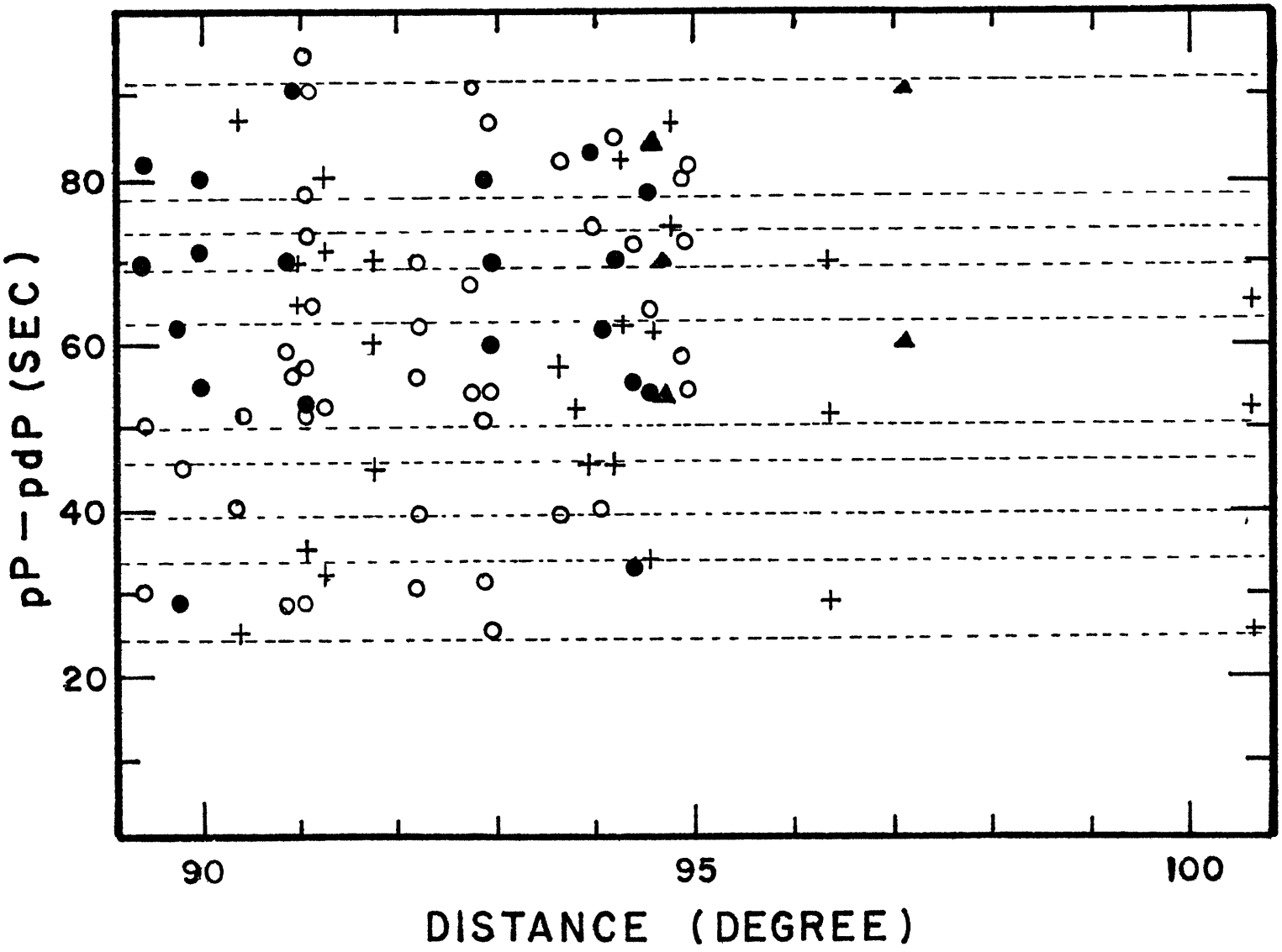
pP − pdP (SEC)
80
60
40
20
90
95
100
DISTANCE (DEGREE)

Figure 12. Examples of precursors to pP at WWSSN stations

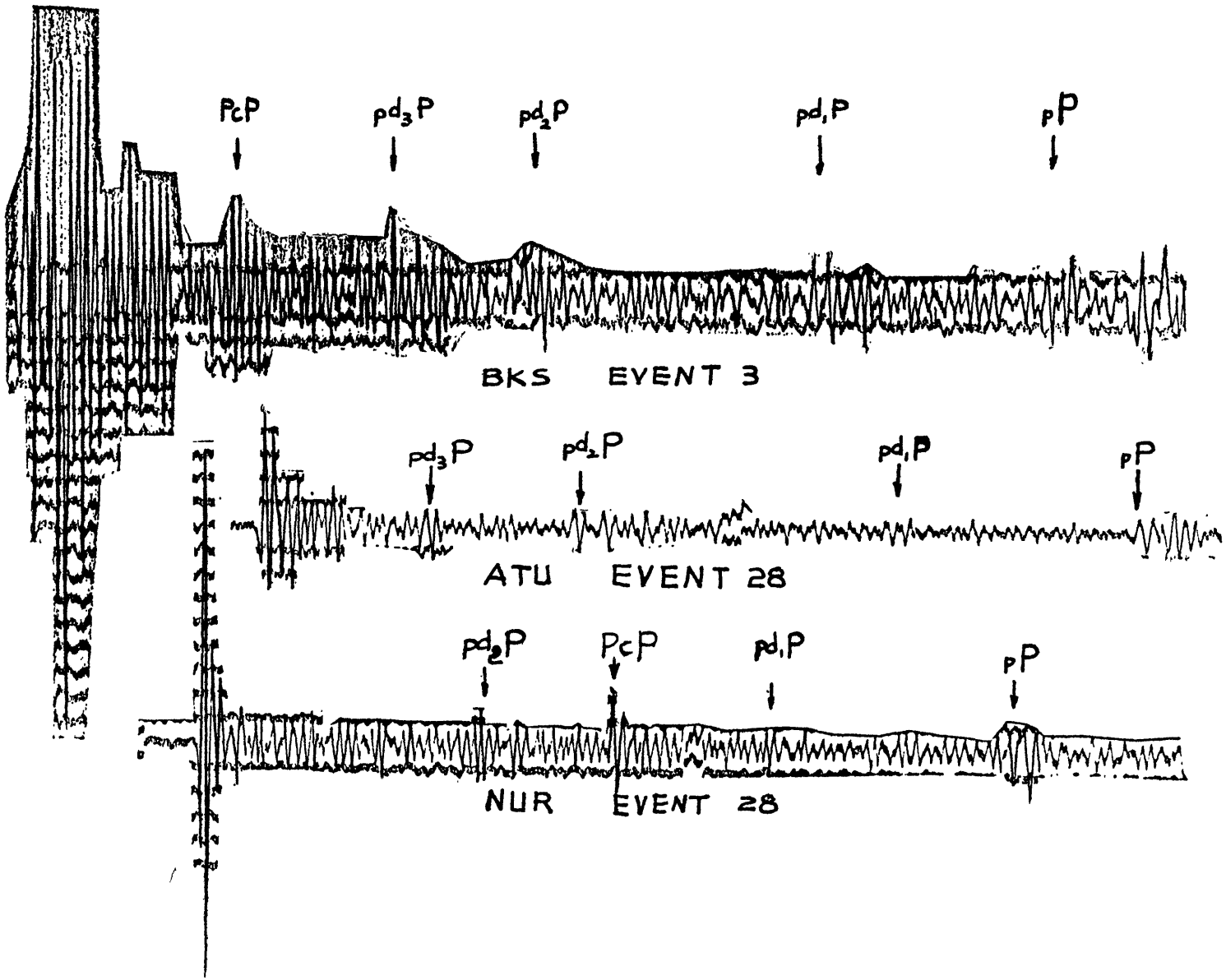
PcP
pd3P
pd2P
pd1P
pP
BKS EVENT 3
pd3P
pd2P
pd1P
pP
ATU EVENT 28
pd2P
PcP
pd1P
pP
NUR EVENT 28

Figure 13. Two simple models used to interpret the depth of the reflectors. The time difference between pP and pdP of events at depth H is approximately equal to that between pP and p of events at depth d.

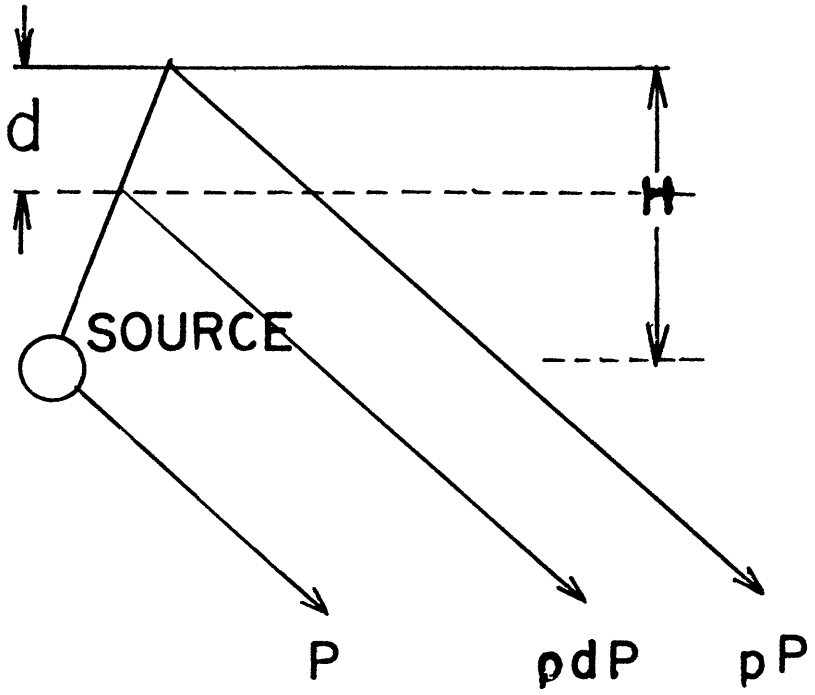
d
H
SOURCE
P
pdP
pP

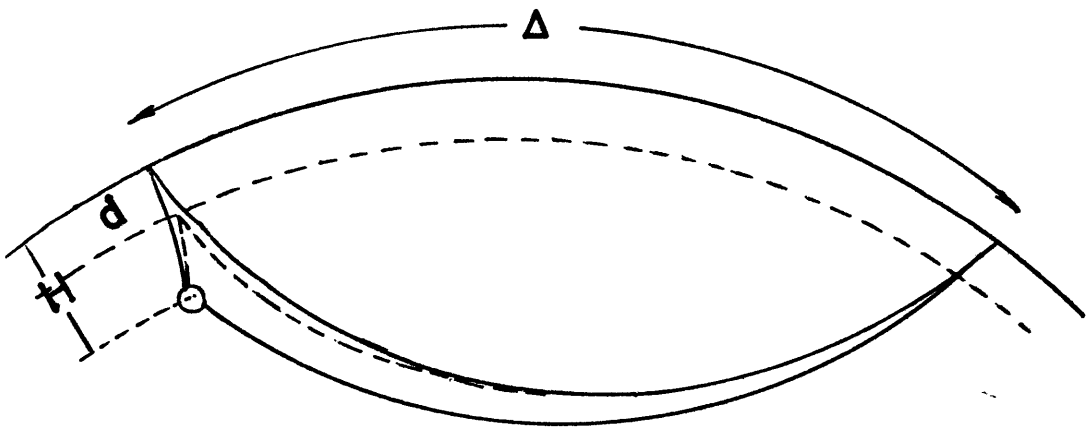
Δ
d
t

Figure 14. The estimated depth of reflectors in South America. Different symbols represent different qualities; solid circle: good, open circle: fair and cross: poor.

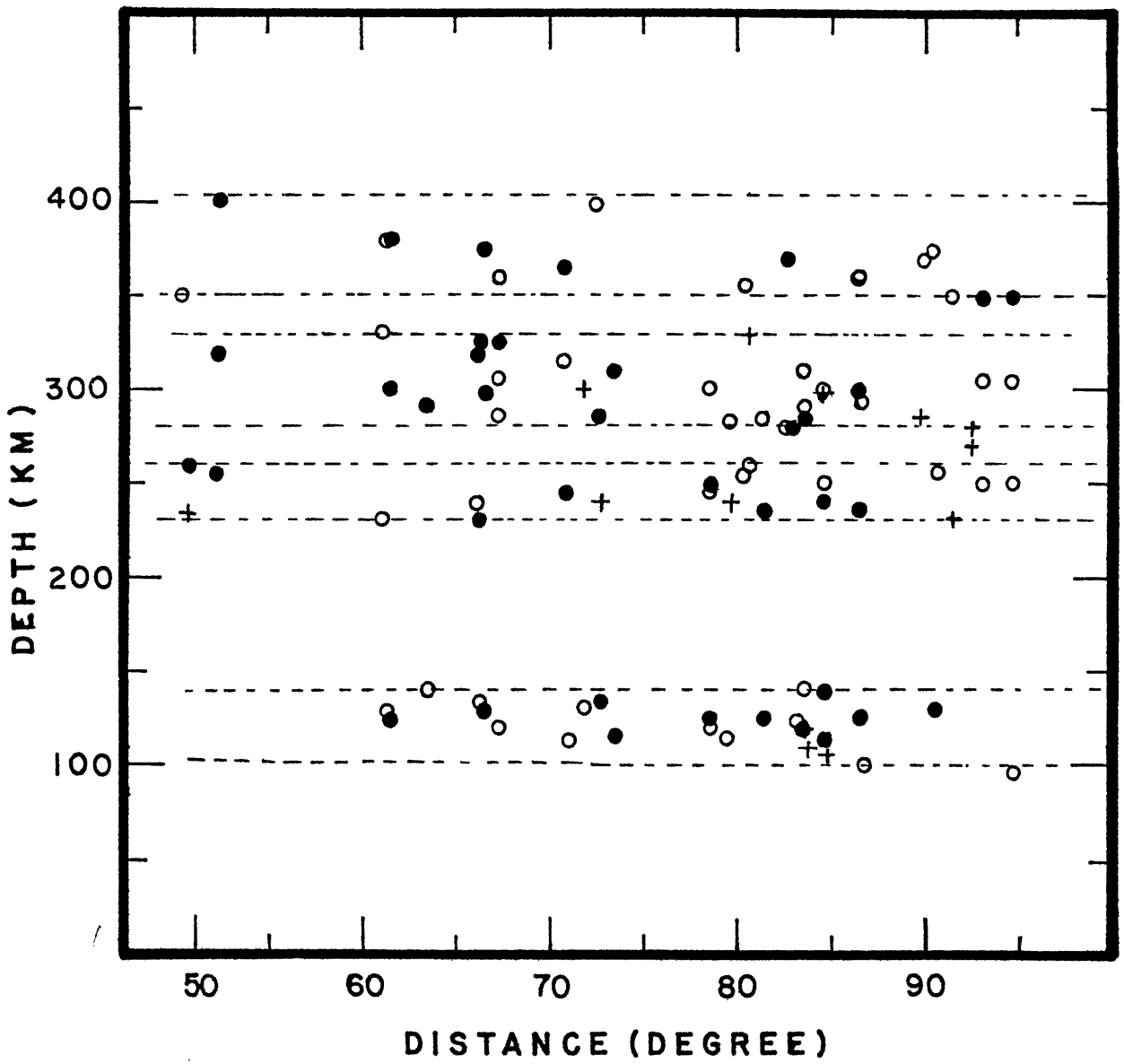
400
300
200
100
DEPTH (KM)
50
60
70
80
90
DISTANCE (DEGREE)

Figure 15. The estimated depth of the reflectors in the Sea of Okhotsk region. Different symbols represent different qualities; solid circle: good, open circle: fair, cross: poor.

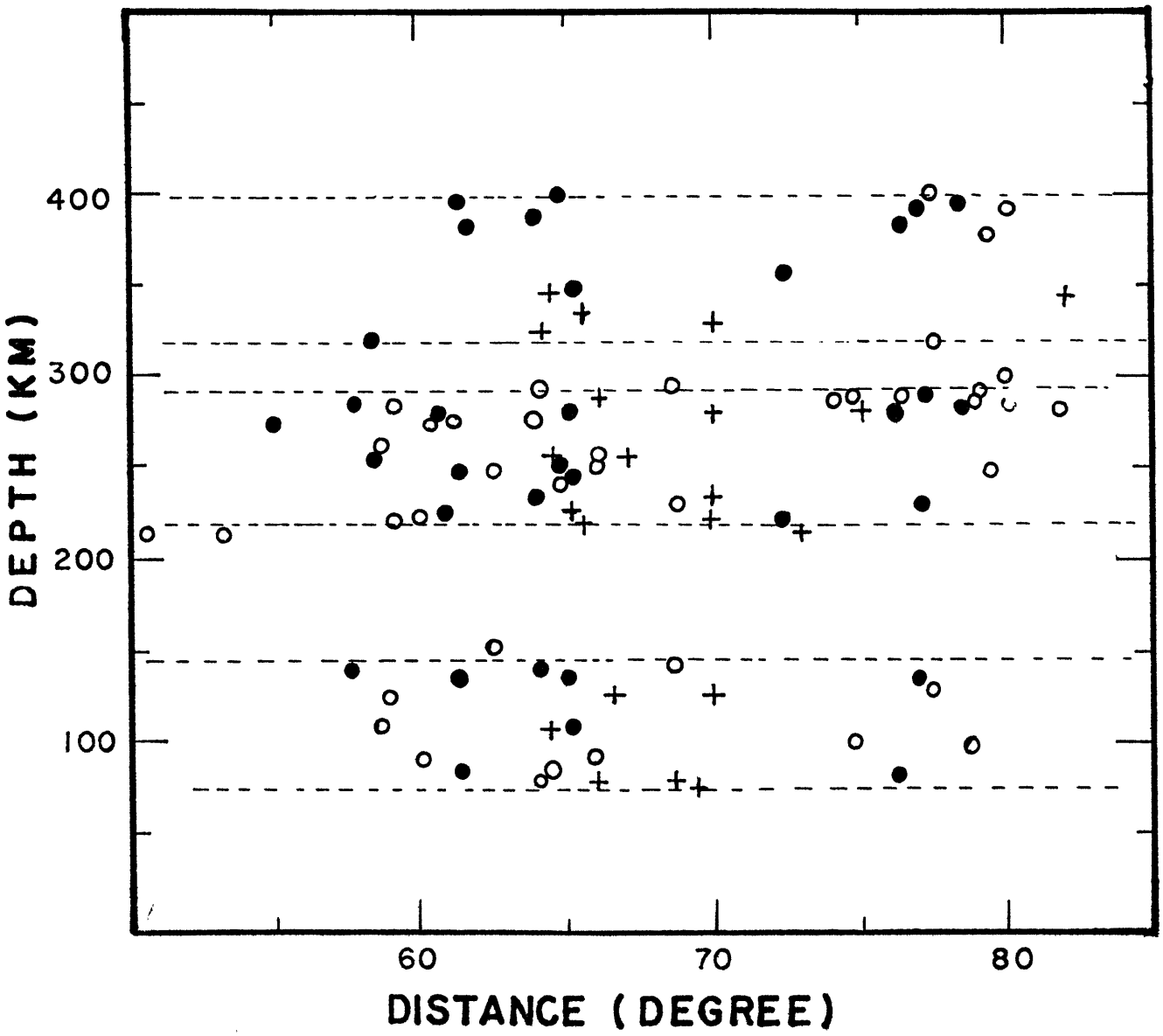
400
300
200
100
DEPTH (KM)
60
70
80
DISTANCE (DEGREE)

Figure 16. The estimated depth of the reflectors in the Bonin Islands region. Different symbols represent different qualities; solid circle: good, open circle: fair, cross: poor.

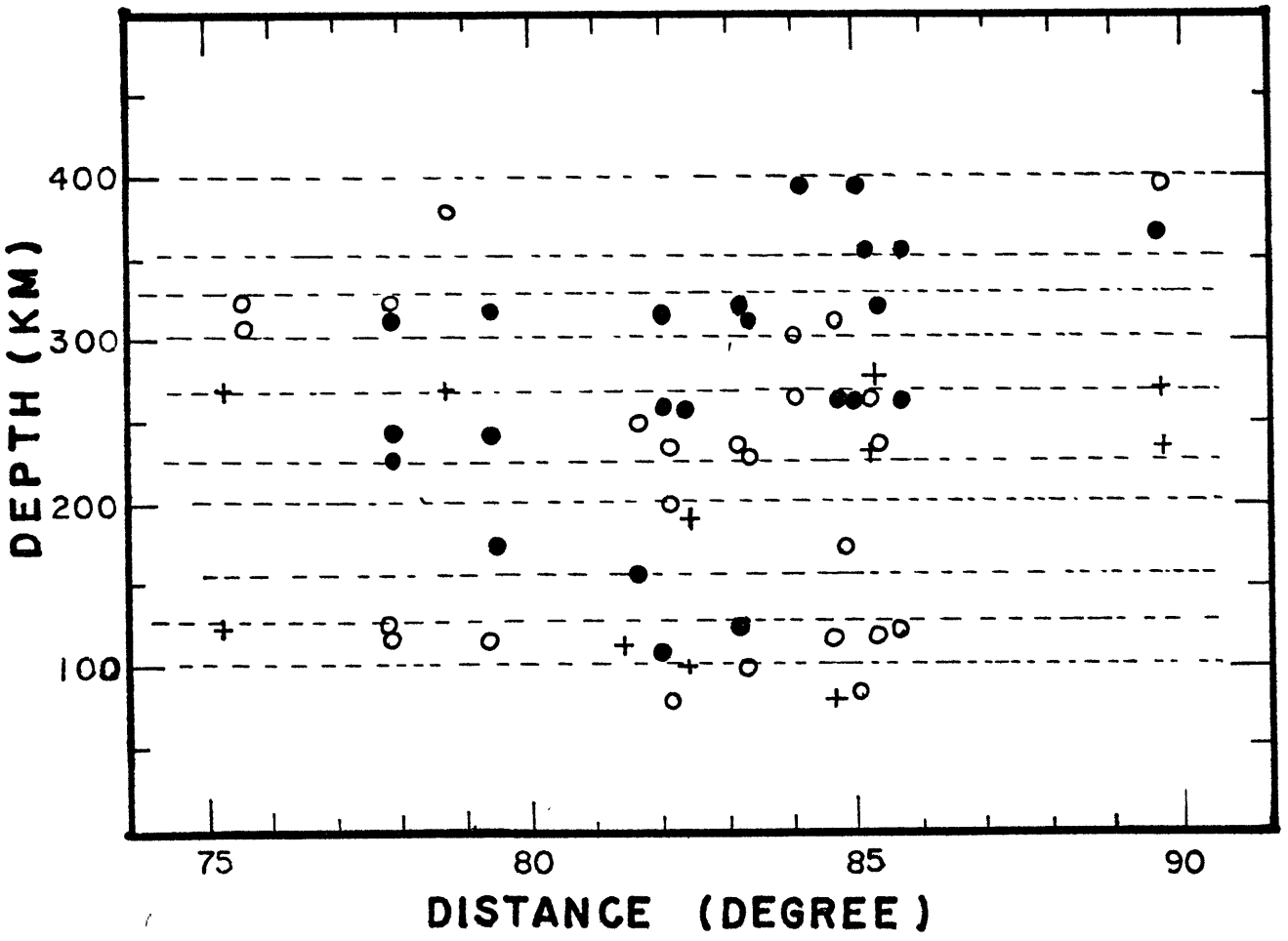
400
300
200
100
DEPTH (KM)
75
80
85
90
DISTANCE (DEGREE)

Figure 17. The estimated depth of the reflectors in the New Hebrides and Fiji-Tonga region. Different symbols represent different qualities; solid circle: good, open circle: fair, cross: poor. The solid trangles are the data in New Hebrides region.

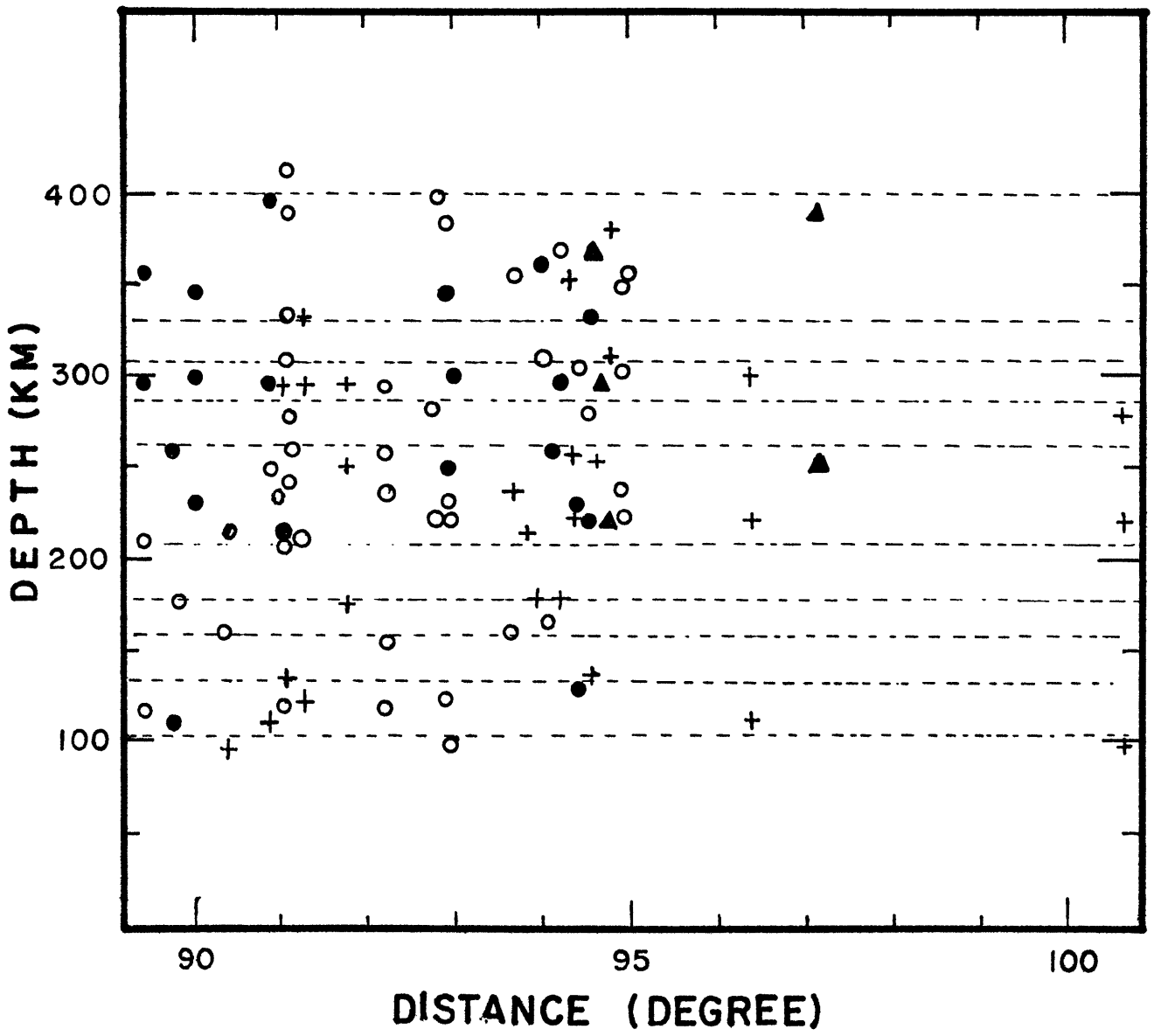
400
300
200
100
DEPTH (KM)
90
95
100
DISTANCE (DEGREE)

Figure 18a. Reflections and refractions of P waves at an interface between two elastic solids.

18b. Reflections and refractions of SV waves at an interface between two elastic solids.

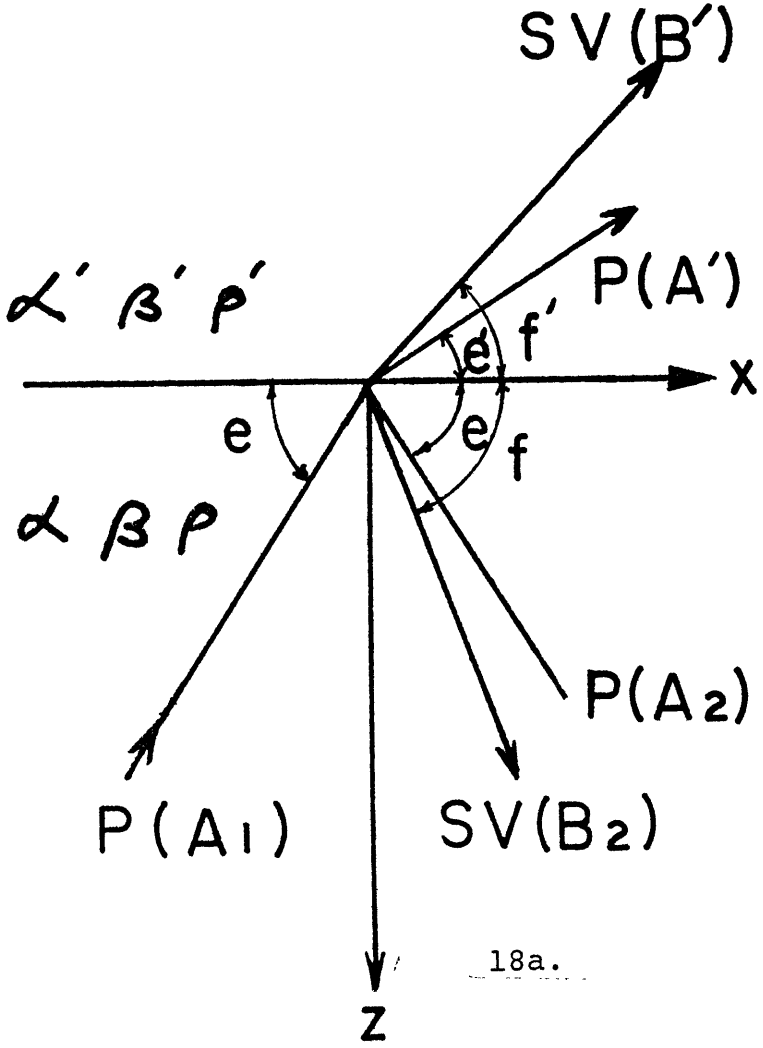
SV(B′)
P(A′)
α′ β′ ρ′
e′
f′
x
e
e
f
α β ρ
P(A2)
P(A1)
SV(B2)
z

18a.

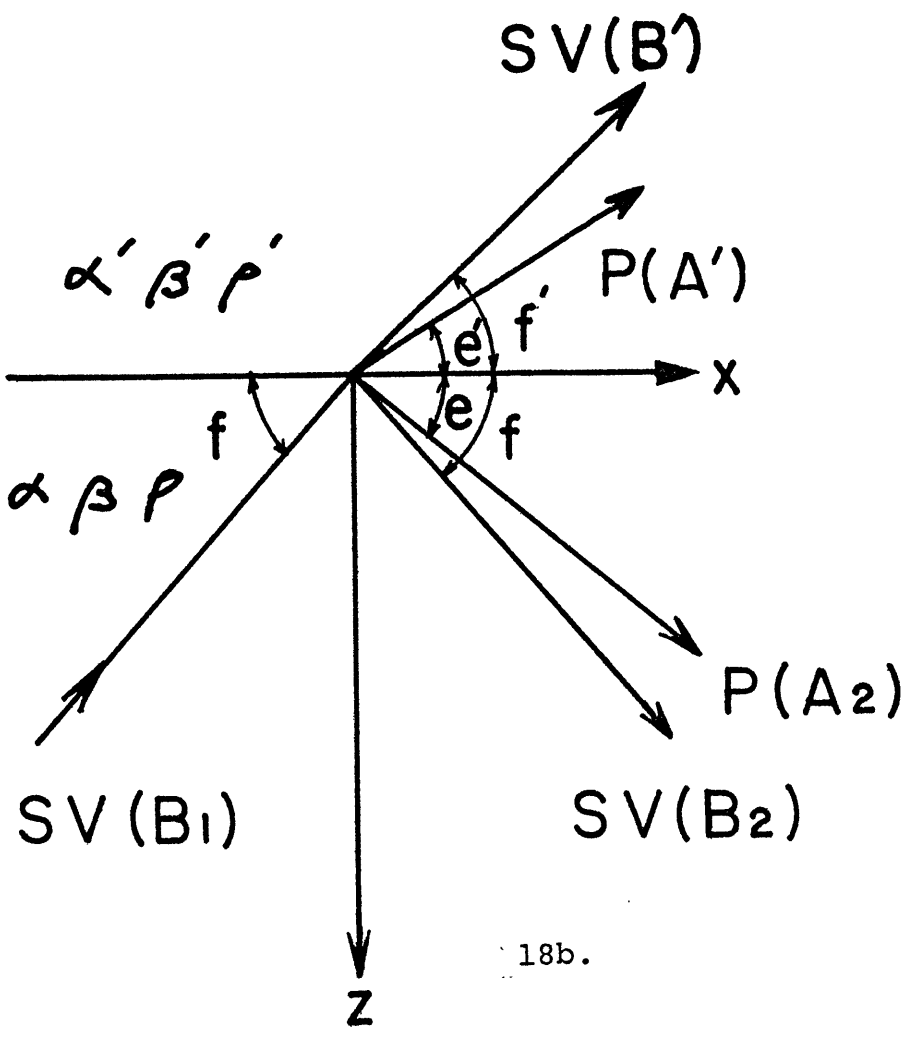
SV(B′)
P(A′)
α′ β′ ρ′
e′
f′
x
e
f
f
α β ρ
P(A2)
SV(B1)
SV(B2)
z

18b.

Figure 19. Reflectors and ray paths of a four layer model.

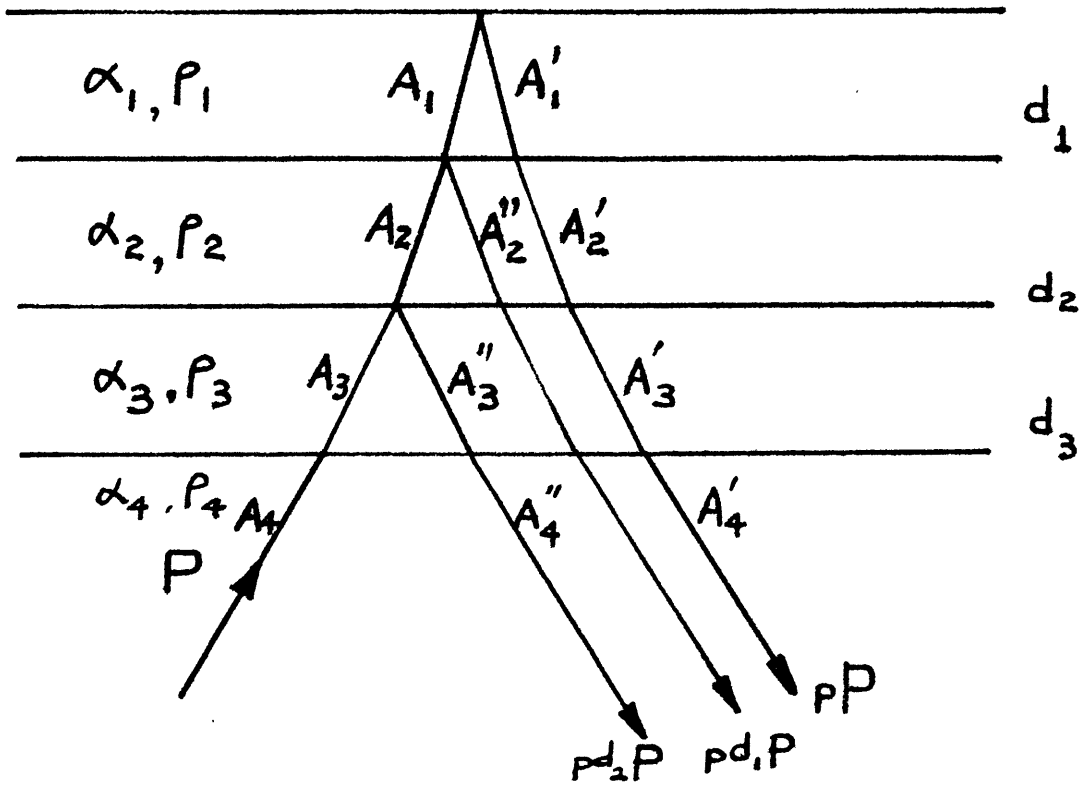
α_1, ρ_1
A_1
A_1'
d_1
α_2, ρ_2
A_2
A_2''
A_2'
d_2
α_3, ρ_3
A_3
A_3''
A_3'
d_3
α_4, ρ_4
A_4
A_4''
A_4'
P
PP
Pd_2P
Pd_1P

Figure 20. Example of P wave converted from SV source at discontinuity. Short period record are recorded at ARE of event 14.

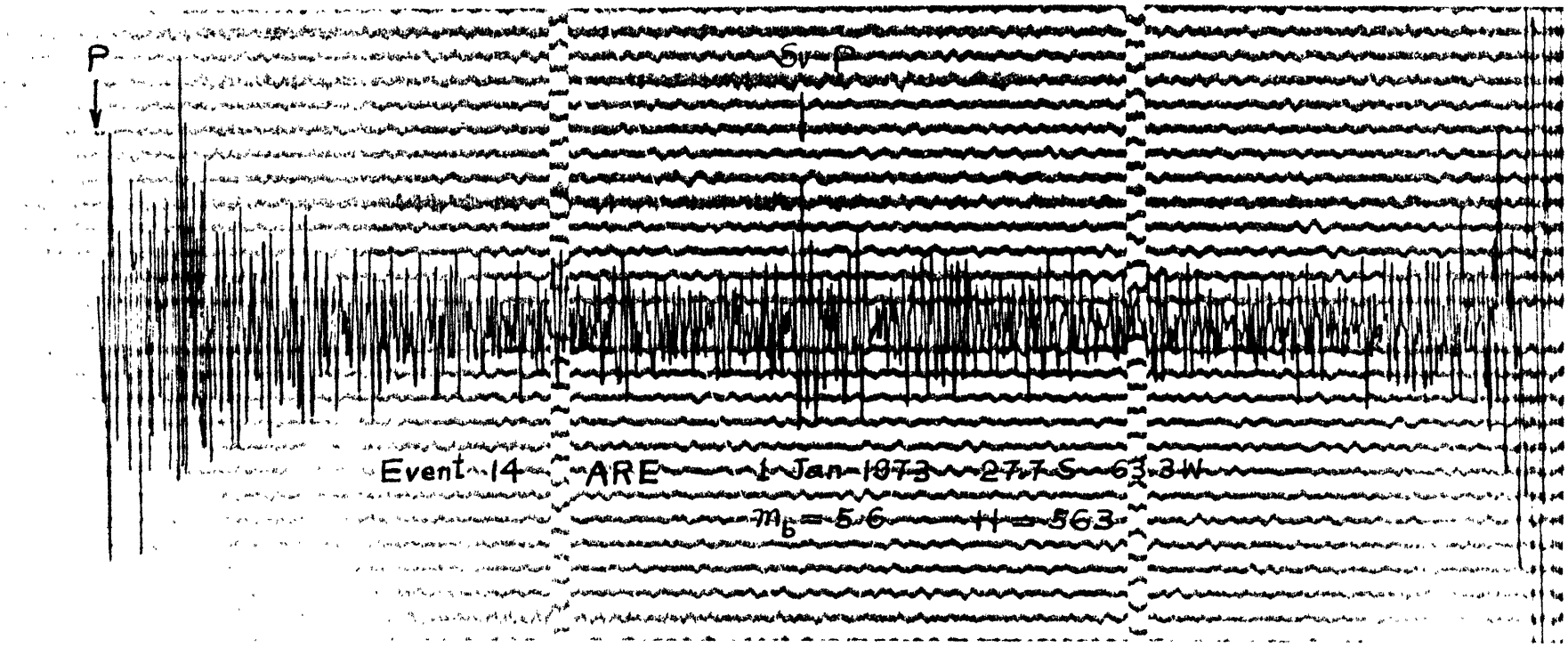
P
Sv P
Event 14 ARE 1 Jan 1973 27.7 S 63.3 W
m_b = 5.6 11 = 563

Figure 21. Seismicity distribution with depth in Chile and Argentina, Peru and West Brazil, New Hebrides, Sea of Okhotsk, Bonin Islands and Central Tonga.

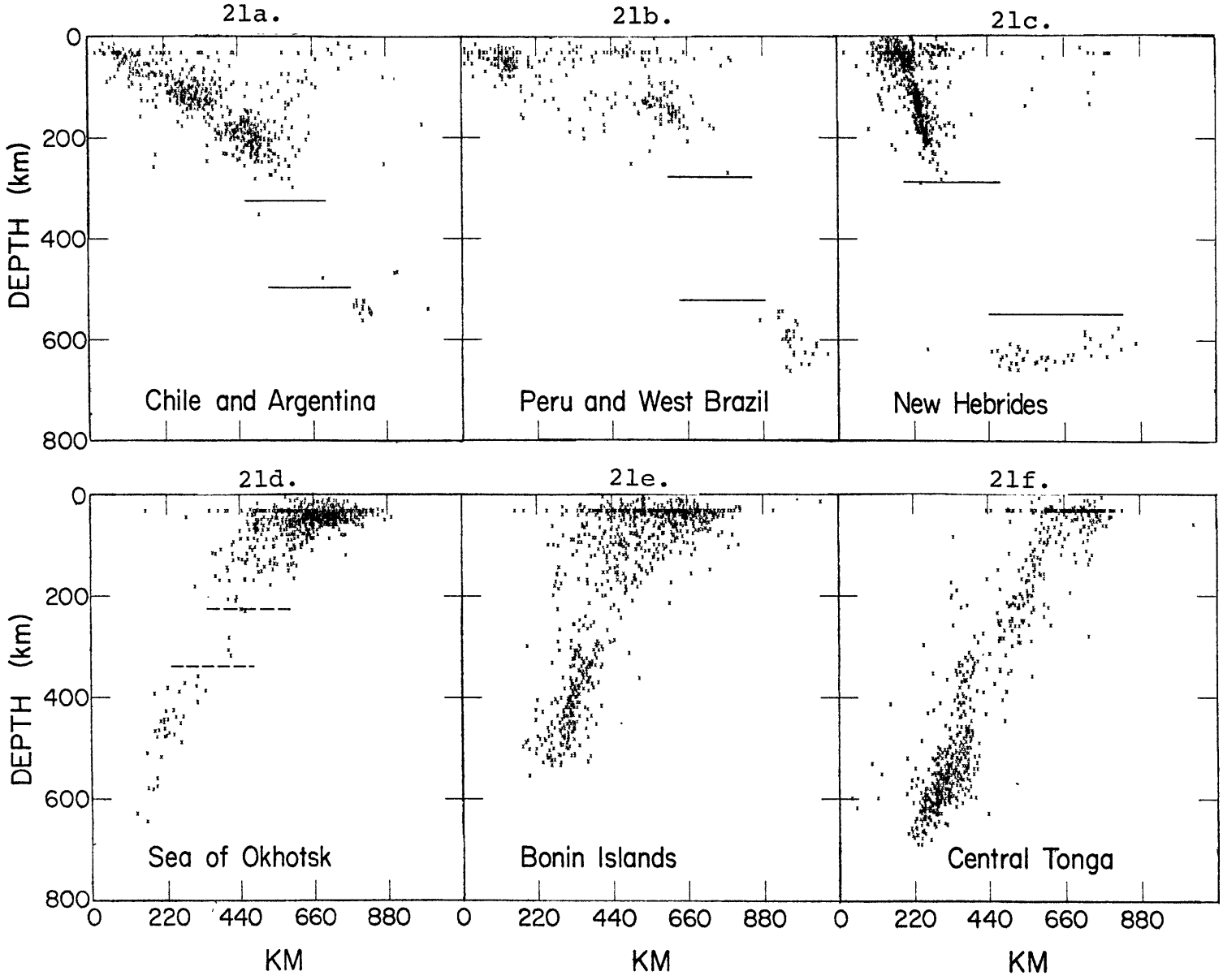
21a.
21b.
21c.
21d.
21e.
21f.
DEPTH (km)
0
200
400
600
800
Chile and Argentina
Peru and West Brazil
New Hebrides
Sea of Okhotsk
Bonin Islands
Central Tonga
0
220
440
660
880
KM

REFERENCES

Adams, R.D., Early reflections of P'P' as an indication of upper mantle structure, Bull. Seismol. Soc. Amer., 58, 1933-1947, 1968.

Adams, R.D., Reflections from discontinuities beneath Antarctica, Bull. Seismol. Soc. Amer., 61, 1441-1451, 1971.

Aki, K., Scattering of P waves under the Montana Lasa, J. Geophys. Res., 78, 1334-1346, 1973.

Angoran, Y.E. and D. Davis, Studies of PP and precursors to it, EOS, 53, 447, 1972.

Anderson, D.L. and C. Sammis, Partial melting in the upper mantle, Phys. Earth Planet. Interiors, 3, 41-50, 1970.

Bolt, B.A., M. O'Neill and A. Qamar, Seismic waves near 110°: Is the structure in core or mantle responsible?, Geophys. J. R. Astr. Soc., 16, 475-487, 1968.

Bolt, B.A. and A. Qamar, Comments on a paper by C. Wright and K.J. Muirhead, "Longitudinal waves from the Novaya Zemlya nuclear explosion of October 27, 1966, recorded at the Warramunga Seismic Array," J. Geophys. Res., 74, 6049-8051, 1969.

Bolt, B.A., PdP and PkikP waves and diffracted PcP waves, Geophys. J. R. Astr. Soc., 20, 367-382, 1970.

Bolt, B.A. and A. Qamar, Observations of pseudo-aftershocks from underground nuclear explosion, Phys. Earth Planet. Interiors, 5, 400-402, 1972.

Burg, J.P., Three dimensional filtering with an array of seismometers, Geophysics, 29, 693-713, 1964.

Capon, J., R.J. Greenfield, and R.J. Kolker, Multidimensional maximum-likelihood processing of a large aperture seismic array, Proc. IEEE, 55, 192-211, 1967.

Capon, J., R.J. Greenfield, R.J. Kolker, and R.T. Lacoss, Short period signal processing results for the large aperture seismic array, Geophysics, 33, 452-472, 1968.

Capon, J., High resolution frequency-wavenumber spectrum analysis, Proc. IEEE, 57, 1408-1418, 1969a.

Capon, J., Investigation of long-period noise at the large aperture seismic array, J. Geophys. Res., 74, 3182-3194, 1969b.

Capon, J., Signal processing and frequency-wavenumber spectrum analysis for a large aperture seismic array, Methods in Computational Physics, 13, Academic Press, New York, 1973.

Capon, J., Characterization of crust and upper mantle structure under LASA as a random medium, Bull. Seismol. Soc. Amer., 64, 235-266, 1974.

Davis, D., J.R. Filson, and E.J. Kelly, Vespa process for analysis of seismic signals, Nature, 232, 8-13, 1971.

Davis, D., Seismology with large arrays, Rep. Prog. Phys., 36, 1233-1283, 1973.

Engdahl, E.R., and E.A. Flinn, Seismic waves reflected from discontinuities within the Earth's upper mantle, Science, 163, 177-179, 1969a.

Engdahl, E.R., and E.A. Flinn, Remarks on the paper 'Early reflections of P'P' as an indication of upper mantle structure,' Bull. Seismol. Soc. Amer., 59, 1415-1418, 1969b.

Engdahl, E.R., and E.P. Flinn, Nature of travel-time anomalies at LASA, J. Geophys. Res., 76, 2706-2715, 1971.

Ewing, M., W.S. Jardetsky, and F. Press, Elastic Waves in Layered Media, McGraw-Hill, New York, 1957.

Frasier, C.W., Massachusetts Institute of Technology, Lincoln Laboratory, Semi-annual Technical Summary, June 30, 1972.

Gutowski, P.R., and E.R. Kanasewich, Velocity spectral evidence of upper mantle discontinuities, Geophys. J. R. Astr. Soc., 36, 21-32, 1974.

Green, P.E., Jr., E.J. Kelly, Jr., and M.J. Levin, A comparison of seismic array processing methods, Geophys. J. R. Astr. Soc., 11, 67-84, 1966.

Gutenberg, B., Erdbebenwellen V und VI, Nachr. Akad. Wiss. Grŏttingen, 121-206 and 625-675, 1912.

Gutenberg, B., Waves reflected at the 'surface' of the earth: P'P'P'P', Bull. Seismol. Soc. Amer., 50, 71-78, 1960.

Hale, A.L., and J.L. Roberts, The Zoeppritz amplitude equations: more errors, Bull. Seismol. Soc. Amer., 64, 285, 1974.

Husebye, E., and R. Madariaga, The origin of precursors to core waves, Bull. Seismol. Soc. Amer., 60, 939-952, 1970.

Isacks, B, and P. Molnar, Distribution of stresses in the descending lithosphere from a global survey of focal mechanism solutions of mantle earthquakes, Rev. Geophys. Space Phys., 9, 103-174, 1971.

Johnson, L.R., Array measurement of P velocities in the upper mantle, J. Geophys. Res., 72, 6309-6325, 1967.

Kanamori, H., Upper mantle structure from apparent velocities of P waves recorded at Wakayama Micro-Earthquake Observatory, Bull. Earthquake Res. Inst. Tokyo Univ., 45, 657-678, 1967.

Lacoss, R.T., E.J. Kelly, and M.N. Toksöz, Estimation of seismic noise structure using arrays, Geophysics, 34, 21-38, 1969.

McCamy, K., R.P. Meyer, and T.J. Smith, Generally applicable solutions of zoeppritz' amplitude equations, Bull. Seismol. Soc. Amer., 52, 923-955, 1962.

Ringwood, A.E., The pyroxene-garnet transformation in the earth's mantle, Earth Planet. Sci. Letters, 2, 255-263, 1967.

Ringwood, A.E., Phase transformations and the constitution of the mantle, Phys. Earth Planet. Interiors, 3, 109-155, 1970.

Ringwood, A.E., and A. Major, The system Mg_2SiO_4-Fe_2SiO_4 at high pressures and temperature, Phys. Earth Planet. Interiors, 3, 89-108, 1970.

Simpson, D.W., C. Wright, and J.R. Cleary, A double discontinuity in the upper mantle, Nature, Physical Science, 231, 201-203, 1971.

Singh, S.J., A. Ben-Menahem and M. Shimshoui, Comments in papers by Costain et al. and McCamy et al. on the solution of Zoeppritz' amplitude equations, Bull. Seismol. Soc. Amer., 60, 277-280, 1970.

Sleep, N., Deep structure and geophysical processes beneath island arcs, Ph.D. Thesis, Massachusetts Institute of Technology, 1972.

Whitcomb, J.H. and D.L. Anderson, Reflection of P'P' seismic waves from discontinuities in the mantle, J. Geophys. Res., 75, 5713-5728, 1970.

Whitcomb, J.H., Asymmetric p'p'-an alternative to P'dP' reflections, Bull. Seismol. Soc. Amer., 63, 133-143, 1973.

Wright, C., and K.J. Muirhead, Longitudinal waves from the Novaya Zemlya nuclear explosion of October 27, 1966, recorded at the Warramunga Seismic Array, J. Geophys. Res., 74, 2034-2048, 1969.

Wright, C., P wave investigations of the Earth's structure using the Warramunga Seismic Array, Ph.D. Thesis, Australian National University, Canberra, 1970.

Wright, C., Array studies of seismic waves arriving between P and PP in the distance range 90° to 115°, Bull. Seismol. Soc. Amer., 62, 385-400, 1972.